

1  
2  
3  
4 Postprint of: Pasika V., Nosko P., Nosko O., Bashta O., Heletiy V., Melnyk V., A method to synthesise groove cam Geneva  
5 mechanisms with increased dwell period, PROCEEDINGS OF THE INSTITUTION OF MECHANICAL ENGINEERS PART C-  
6 JOURNAL OF MECHANICAL ENGINEERING SCIENCE (2024). Copyright 2024 IMechE. DOI: [10.1177/09544062241234477](https://doi.org/10.1177/09544062241234477)  
7  
8  
9  
10  
11  
12  
13  
14  
15  
16  
17  
18

1

19 A method to synthesise groove cam Geneva mechanisms with increased dwell period

20  
21 Viacheslav Pasika<sup>a</sup>, Pavlo Nosko<sup>b</sup>, Oleksii Nosko<sup>c\*</sup>, Oleksandr Bashta<sup>b</sup>, Volodymyr Heletiy<sup>a</sup>,  
22 Volodymyr Melnyk<sup>b</sup>  
23

24  
25 <sup>a</sup> Lviv Polytechnic National University,  
26 Department of Technical Mechanics and Dynamics of Machines, Bandery 32, Lviv, 79013, Ukraine

27 <sup>b</sup> National Aviation University, Aerospace Faculty, Department of Applied Mechanics and  
28 Materials Engineering, Lubomyr Husar 1, Kyiv, 03058, Ukraine

29 <sup>c</sup> Gdansk University of Technology, Faculty of Mechanical Engineering and Ship Technology,  
30 Narutowicza 11/12, Gdansk, 80233, Poland

31 \*Corresponding author: [oleksii.nosko@pg.edu.pl](mailto:oleksii.nosko@pg.edu.pl), <https://orcid.org/0000-0002-5259-1426>  
32  
33  
34

35 Abstract

36 The present study develops a method to synthesise the groove cam Geneva mechanism with  
37 increased dwell period. The main condition of the synthesis is to provide the desired law of motion  
38 of the wheel. Additional synthesis conditions are the limitation of the maximum pressure angle and  
39 the limitation of the minimum curvature radius of the cam profile. Unlike the conventional Geneva  
40 mechanisms, the synthesised groove cam Geneva mechanisms enable motion of the wheel due to an  
41 arbitrarily specified law, double locking of the wheel at its dwell-to-motion and motion-to-dwell  
42 transitions, absence of soft impacts in the extreme positions. The analysis shows that for the  
43 cycloidal law of motion, number of slots in range 3 to 15 and additional dwell coefficient in range 0  
44 to 0.7, the operating time coefficient can be provided in wide range from 0.053 to 0.765. The  
45 effectiveness of the method is illustrated by numerical examples.  
46  
47

48 Keywords: Geneva mechanism, groove cam Geneva mechanism, synthesis method, number of  
49 wheel slots, operating time coefficient, additional dwell coefficient  
50  
51  
52  
53  
54  
55  
56  
57  
58  
59  
60

## Notation

$a_k$	wheel rotation invariant
$b_k$	wheel angular velocity invariant
$c_k$	wheel angular acceleration invariant
$k$	dimensionless time
$k_{at}$	additional dwell coefficient
$k_w$	operating time coefficient
$l_{AB}$	distance between the wheel axis and driving pin axis
$l_{OA}$	initial crank radius
$l_{OB}$	distance between the crank rotation axis and wheel axis
$r$	crank radius
$t_s$	wheel dwell period
$t_t$	wheel motion period
$z$	number of slots
$\lambda_2$	dimensionless distance between the wheel axis and driving pin axis
$\lambda_a$	dimensionless distance between the crank rotation axis and wheel axis
$\lambda_r$	dimensionless crank radius
$\lambda_{r1, \dots, \lambda_{r4}}$	dimensionless crank radius in the zones I, ..., IV
$\lambda_{rc}$	dimensionless limiting radius
$\nu$	pressure angle
$\nu_{max}$	maximum pressure angle
$[\nu]$	allowable pressure angle
$\rho_{min}$	dimensionless minimum curvature radius of the cam profile
$[\rho]$	dimensionless allowable curvature radius of the cam profile
$\varphi_1$	crank rotation angle
$\varphi_2$	wheel rotation angle
$\varphi_{1\Sigma}$	total crank rotation angle
$\varphi_{2\Sigma}$	total wheel rotation angle
$\omega_1$	crank angular velocity
$\omega_2$	wheel angular velocity
$\Delta\varphi$	additional dwell angle

## 1. Introduction

Increasing speeds and productivity of automatic machines require employment of highly functional and efficient cyclic mechanisms. Geneva mechanisms belong to the cyclic mechanisms commonly used in automatic machines [1–3]. Their application range is extensive and has evolved from mechanical watches and motion-picture projectors to discrete motion drives in robotic manipulators and CNC machines [4–10].

The Geneva mechanisms are simple, technological and undemanding in maintenance. However, like all lever mechanisms, they possess certain disadvantages. First of all, the laws of motion of the wheel are characterised by impact phenomena in its extreme positions, which imposes speed and energy limitations. Moreover, in the Geneva mechanism with a constant crank radius and a fixed number  $z$  of slots on the wheel, the operating time coefficient  $k_w = t_t/t_s$  equal to the ratio of the motion period  $t_t$  of the wheel to its dwell period  $t_s$  is governed by the number  $z$  as per the equality  $k_w = (z - 2)/(z + 2)$ . Adjusting the coefficient  $k_w$  by changing the number  $z$  is not feasible in many practical cases [11].

There is a class of automatic machines and automated lines employing the Geneva mechanism where most technological operations are performed when the wheel is stationary. This class includes but is not limited to engine lathe machines, carousel lathe machines, cutting machines, milling machines, drilling machines, packaging machines, conveyor machines, lining machines. For example, if the Geneva mechanism is used in a bottle filling machine, rotation of the wheel provides placing the consecutive empty bottle under the valve, whilst filling of the bottle with liquid takes place during the dwell period  $t_s$ . The productivity of such automatic machines can be thus improved by reducing the motion period  $t_t$  or, in other words, increasing the dwell period  $t_s$ . However, if large inertial masses are attached to the wheel, the motion period  $t_t$  cannot be reduced without a significant increase in the wheel angular acceleration and, accordingly, inertial loads.

Further, the disadvantages of the Geneva mechanisms include the fact that the wheel is locked solely by a locking ring [12]. As the driving pin of the crank enters the slot, the edge of the locking ring, which is rigidly connected to the crank, comes out of contact with the wheel. High accuracy should be, therefore, guaranteed for the mutual location between the crank and locking ring. Errors in the manufacture and installation of the mechanism and its wear lead to the occurrence of unwanted gaps. This, in its turn, results in non-simultaneous entry of the driving pin into the slot and exit of the locking ring from contact, which is accompanied by increased impact loads. A similar situation is observed when the driving pin leaves the slot.

Several approaches have been proposed to improve the dynamic performance of the Geneva mechanisms. The first approach implies application of compound mechanisms to eliminate soft impacts (discontinuous accelerations) in the extreme positions [13–22]. Two or more mechanisms are connected in series so that the angular acceleration of the wheel changes continuously during its motion. This approach inevitably introduces extra components to the system. The second approach is using damping elements in the Geneva mechanism in order to reduce the impact loads [23, 24], which also leads to extra components in the system. The third approach is to modify the geometry of the slots [25–29]. Curvilinear slots are designed to provide the desired law of motion, similarly as in cam mechanisms. Although processing of the curvilinear slots is resource consuming, the approach enables adjusting the dwell period  $t_s$  even for a fixed number  $z$  of slots.

The study [30] investigates the applicability of the wheel with barrel-shaped slots, called ‘Quickermittent’, for motion picture film projectors. Such a mechanism allows to reduce the indexing time whilst maintaining control over the loads on the film and mechanism itself. However, due to the fact that the slot is wider in its middle part, the driving pin can hit the walls of the slot, which affects adversely on the motion stability, especially at low rotational speeds. In addition, Quickermittent mechanisms tend to be noisier than the Geneva mechanisms.

A double-pins without locking arc Geneva mechanism is developed in the study [31]. The proposed mechanism has two driving pins in contrast to the conventional Geneva mechanism with one driving pin, resulting in two times higher angular velocity of the wheel. Smaller impact loads in

the mechanism are achieved by optimising the transitional part of the slot, which implies, however, higher manufacturing costs.

The studies [2, 8, 32, 33] suggest that the functionality of the Geneva mechanism can be substantially extended by introducing a groove cam element. The groove cam Geneva mechanism comprises input crank 1, output wheel 2, groove cam 3, driving pin 4 and roller follower 5, as shown in Fig.1. The crank 1 rotates at constant angular velocity  $\omega_1$  and simultaneously moves radially due to the path of the roller follower 5 along the groove of the cam 3. The driving pin 4 on the crank 1 brings the wheel 2 in motion. Thus, the mechanism makes use of the cam 3 to control the radius of action of the driving pin 4, which provides the necessary kinematic characteristics of the wheel 2.

[insert Figure 1.]

The analysis of the above-mentioned studies indicates a lack of research devoted to solving the problem of synthesising the groove cam Geneva mechanism and analysing the influence of different parameters on its performance. The purpose of the present study is to develop a method to synthesise the groove cam Geneva mechanism with increased dwell period that satisfies the desired law of motion of the wheel (main condition), allowable pressure angle and allowable curvature radius of the cam profile (additional conditions). The following tasks are solved to achieve this purpose: development of the general approach to determining the path of the driving pin due to the specified operating time coefficient  $k_w$  (Section 2); formulation of the additional conditions of synthesis (Section 3); development of the method to synthesise the driving pin path (Section 4); development of the synthesis algorithm (Section 5); illustration of the method application (Section 6).

## 2. General approach to determining the driving pin path

A detailed schematic of the groove cam Geneva mechanism is shown in Fig.2. The numbering of the elements in the schematic corresponds to Fig.1. In addition to the input crank 1, output wheel 2, groove cam 3, driving pin 4 and roller follower 5, Fig.2 presents the locking ring 6. To reduce the number of parameters in the present study and simplify analysis, the roller follower 5 is assumed to have a common axis with the driving pin 4, i.e. the centre  $C$  of the roller follower 5 coincides with the centre  $A$  of the driving pin 4. Under this assumption, the profile of the cam 3 coincides with the path of the centre  $A$  of the driving pin 4.

[insert Figure 2.]

Imagine that the driving pin 4 enters the slot of the wheel 2 at the moment when the crank 1 and slot are mutually perpendicular. The driving pin 4 passes then along the slot from the position  $A$  to the position  $A_1$ , which corresponds to a certain rotation angle  $\Delta\varphi$  of the crank 1. In this interval, the wheel 2 is stationary due to its locking by the ring 6 and motion of the driving pin 4 along the line  $AA_1$ . As the crank 1 rotates by the angle  $\Delta\varphi$ , the wheel 2 is brought in motion. Apparently, the described situation corresponds to an increase in the dwell period  $t_s$  of the wheel 2. The angle  $\Delta\varphi$  is referred to as 'additional dwell angle'.

There is thus a principal difference between the operation of the conventional Geneva mechanism and that of the groove cam Geneva mechanism. In the former, the locking of the wheel at its dwell-to-motion and motion-to-dwell transitions is performed solely by the locking ring, whereas in the latter it is performed by both locking ring 6 and driving pin 4.

Derive an analytical expression for the operating time coefficient  $k_w$ . Introduce the total crank rotation angle  $\varphi_{1\Sigma}$  and total wheel rotation angle  $\varphi_{2\Sigma}$  as

$$\varphi_{1\Sigma} = \pi \left( 1 - \frac{2}{z} \right);$$

$$\varphi_{2\Sigma} = \frac{2\pi}{z}$$

Further, express the motion period  $t_t$  and dwell period  $t_s$  in the form

$$t_t = \frac{\varphi_{1\Sigma} - 2\Delta\varphi}{\omega_1};$$

$$t_s = \frac{2\pi - \varphi_{1\Sigma} + 2\Delta\varphi}{\omega_1}$$

Based on the equations above, the operating time coefficient  $k_w$  can be expressed as follows:

$$k_w = \frac{t_t}{t_s} = \frac{\pi(z-2)/z - 2\Delta\varphi}{\pi(z+2)/z + 2\Delta\varphi} \quad (1)$$

After defining the additional dwell coefficient as the ratio

$$k_{at} = \frac{2\Delta\varphi}{\varphi_{1\Sigma}}$$

Eq.(1) can be rewritten in the following manner:

$$k_w = \frac{(z-2)(1-k_{at})}{2z - (z-2)(1-k_{at})} \quad (2)$$

Apparently, the operating time coefficient  $k_w$  is reduced at  $\Delta\varphi > 0$  and, accordingly,  $k_{at} > 0$ . As the coefficient  $k_{at}$  tends to 1, the additional dwell angle  $\Delta\varphi$  increases significantly along with the geometric dimensions of the mechanism (see Fig.2). It is reasonable, therefore, to limit  $k_{at}$ , and the present study accepts that  $k_{at} \leq 0.7$ . Due to the fact that the number  $z$  of slots cannot be less than 3, whilst the Geneva mechanisms with  $z > 15$  are rarely met in practice, the number  $z$  is accepted to be in range from 3 to 15.

Fig.3 illustrates the dependence of the operating time coefficient  $k_w$  on the additional dwell coefficient  $k_{at}$  and number  $z$  due to Eq.(2). The analysis shows that for the conventional Geneva mechanism ( $k_{at} = 0$ ), the coefficient  $k_w$  changes from 0.2 to 0.765. By contrast, the groove cam Geneva mechanism has a significantly wider range of the coefficient  $k_w$  from 0.053 to 0.765 at  $0 < k_{at} \leq 0.7$ . Note that the coefficient  $k_w$  is more sensitive to the variation of  $k_{at}$  at smaller values of  $k_{at}$ .

[insert Figure 3.]

Considering Fig.2, introduce the dimensionless crank radius  $\lambda_r$ , dimensionless distance  $\lambda_2$  between the driving pin axis  $A$  and wheel axis  $B$ , dimensionless distance  $\lambda_a$  between the crank rotation axis  $O$  and wheel axis  $B$  as

$$\lambda_r = \frac{r}{l_{OA}};$$

$$\lambda_2 = \frac{l_{AB}}{l_{OA}};$$

$$\lambda_a = \frac{l_{OB}}{l_{OA}} = \frac{1}{\sin(\pi/z)}$$



where  $r$  is the crank radius, i.e. the distance between the crank rotation axis  $O$  and driving pin axis  $A$ ;  $l_{AB}$  is the distance between the driving pin axis  $A$  and wheel axis  $B$ ;  $l_{OB}$  is the distance between the crank rotation axis  $O$  and wheel axis  $B$ ;  $l_{OA}$  is the initial crank radius for the perpendicular position between the crank and slot.

Writing the equation of closed vector circuit in the form

$$\bar{\lambda}_r + \bar{\lambda}_2 = \bar{\lambda}_a$$

and projecting it on the horizontal and vertical axes yield that

$$\lambda_r = \lambda_a \frac{\sin(\pi/z - \varphi_2)}{\cos(\varphi_1 + \varphi_2)}$$

$$\lambda_2 = \lambda_a \frac{\cos(\pi/z + \varphi_1)}{\cos(\varphi_1 + \varphi_2)}$$

(3)

where  $\varphi_1$  and  $\varphi_2$  are the rotation angles of the respective crank and wheel.

Further, represent the rotation angles of the respective crank and wheel in the form

$$\varphi_1 = k\varphi_{1\Sigma};$$

$$\varphi_2 = a_k\varphi_{2\Sigma}$$

where  $k = \varphi_1/\varphi_{1\Sigma}$  is the dimensionless time;  $a_k$  is the wheel rotation invariant. Then the derivatives of the radius  $\lambda_r$  with respect to  $\varphi_1$  read

$$\lambda_r' = \frac{d\lambda_r}{d\varphi_1} = \frac{\lambda_a}{\cos^2(\varphi_1 + \varphi_2)} \left( \sin(\varphi_1 + \varphi_2) \sin\left(\frac{\pi}{z} - \varphi_2\right) - \varphi_2' \cos\left(\frac{\pi}{z} + \varphi_1\right) \right);$$

$$\lambda_r''$$

$$= \frac{d^2\lambda_r}{d\varphi_1^2} = -\frac{\lambda_a}{\cos^3(\varphi_1 + \varphi_2)} \left( \varphi_2'' \cos(\varphi_1 + \varphi_2) \cos\left(\frac{\pi}{z} + \varphi_1\right) + 2\varphi_2' \left( (1 + \varphi_2') \cos(\varphi_1 + \varphi_2) \sin\left(\frac{\pi}{z} + \varphi_1\right) - (2 + \varphi_2') \sin\left(\frac{\pi}{z} - \varphi_2\right) \right) + (1 + \sin^2(\varphi_1 + \varphi_2)) \sin\left(\frac{\pi}{z} - \varphi_2\right) \right)$$

(4)

with

$$\varphi_2' = \frac{d\varphi_2}{d\varphi_1} = b_k \frac{\varphi_{2\Sigma}}{\varphi_{1\Sigma}};$$

$$\varphi_2'' = \frac{d^2\varphi_2}{d\varphi_1^2} = c_k \frac{\varphi_{2\Sigma}}{\varphi_{1\Sigma}^2}$$

(5)

where  $b_k = da_k/dk$  and  $c_k = db_k/dk$  are the wheel angular velocity and acceleration invariants.

Thus, as the crank radius  $\lambda_r$  changes due to Eq.(3), the wheel moves according to the prescribed law with rotation invariant  $a_k$ . Remember that the expressions for  $\lambda_r$ ,  $\lambda_r'$ ,  $\lambda_r''$  given by Eqs.(3)–(5) are valid if the wheel motion starts from the perpendicular position between the crank and slot.

### 3. Additional conditions of synthesis

Since the studied mechanism (see Fig.2) includes a cam mechanism in the form of the roller follower in contact with the groove cam, the additional conditions of synthesis arise, as considered next.

### 3.1. Limitation condition for the maximum pressure angle

In order to prevent jamming in the cam mechanism, the maximum value  $\nu_{\max}$  of the pressure angle

$$\nu = \arctan \frac{\lambda'_r}{\lambda_r} \quad (6)$$

should not exceed the allowable pressure angle  $[\nu]$ . The corresponding condition limiting the maximum pressure angle  $\nu_{\max}$  is formulated as

$$\nu_{\max} \leq [\nu] \quad (7)$$

The allowable pressure angle  $[\nu]$  is chosen depending on the angular velocity and load in the cam mechanism. In most engineering applications, the value of  $[\nu]$  is in range from  $30^\circ$  to  $45^\circ$ . In the present study,  $[\nu]$  is accepted to be between  $32.5^\circ$  and  $41.6^\circ$ , which corresponds to the case of rotary tables like Vertex Precision Tilting Rotary Table VUT used in carousel lathe machines, cutting machines, milling machines, drilling machines and conveyor machines [33].

### 3.2. Limitation condition for the minimum curvature radius of the cam profile

In order to prevent sharpening and interference of the cam profile, it is necessary to limit from below its minimum curvature radius  $\rho_{\min}$ . The allowable curvature radius  $[\rho]$  of the cam profile is determined by the dimensionless expression [34]

$$[\rho] = \max \left\{ \frac{\lambda'_r}{\tan [\nu]} - \lambda_r + \min \lambda_r \right\} \quad (8)$$

The minimum curvature radius  $\rho_{\min}$  of the cam profile is derived from the known formula for the radius of curvature given in polar coordinates as

$$\rho_{\min} = \min \left\{ \frac{(\lambda_r^2 + (\lambda'_r)^2)^{3/2}}{\lambda_r^2 + 2(\lambda'_r)^2 - \lambda_r \lambda''_r} \right\} \quad (9)$$

The condition limiting the minimum curvature radius  $\rho_{\min}$  takes then the following form:

$$\rho_{\min} \geq [\rho] \quad (10)$$

Thus, the additional conditions of synthesis include Eq.(7) limiting the maximum pressure angle  $\nu_{\max}$  and Eq.(10) limiting the minimum curvature radius  $\rho_{\min}$  of the cam profile.

## 4. Method to synthesise the driving pin path

Fig.4 shows the characteristic zones of the crank motion: I — linear path of the driving pin, stationary wheel; II — path of the driving pin for the wheel motion period; III — linear path of the driving pin, stationary wheel; IV — path of the driving pin which provides a smooth conjugation of the end of the zone III and the start of the zone I. The crank radius  $\lambda_r$  is determined next for each zone.

[insert Figure 4.]

Zone I starts in the position A when the driving pin enters the slot, and it ends in the position  $A_1$  when the crank rotates by the additional dwell angle  $\Delta\varphi$ . The rotation angle  $\varphi_1$  of the crank



changes, thereby, from 0 to  $\Delta\varphi$ . Considering the fact that the wheel is stationary, i.e.  $\varphi_2 = 0$ , a simplified expression for the crank radius  $\lambda_{r1}$  is derived in the form

$$\lambda_{r1} = \frac{1}{\cos \varphi_1} \quad (11)$$

*Zone II* starts in the position  $A_1$  and ends in the position  $A'_1$ . The wheel moves according to the prescribed law. The crank rotation angle  $\varphi_1$  changes from  $\Delta\varphi$  to  $(\varphi_{1\Sigma} - \Delta\varphi)$ . The crank radius  $\lambda_{r2}$  is found from Eqs.(3)–(5).

*Zone III* starts in the position  $A'_1$  and ends in the position  $A'$ . The motion of the driving pin occurs similarly to that in the zone I. The crank rotation angle  $\varphi_1$  changes from  $(\varphi_{1\Sigma} - \Delta\varphi)$  to  $\varphi_{1\Sigma}$ . Since  $\varphi_2 = \varphi_{2\Sigma} = 2\pi/z$ , the expression for the crank radius  $\lambda_{r3}$  reads

$$\lambda_{r3} = -\frac{1}{\cos(2\pi/z + \varphi_1)}$$

*Zone IV* starts in the position  $A'$  and ends in the position  $A$ . Accordingly, the crank rotation angle  $\varphi_1$  changes from  $\varphi_{1\Sigma}$  to  $2\pi$ . The crank radius  $\lambda_{r4}$  can be defined in the form of polynomial

$$\lambda_{r4} = \sum_{i=1}^n a_i \varphi_1^{i-1} \quad (12)$$

where  $n$  is the number of the conditions imposed on the crank radius  $\lambda_{r4}$ .

The boundary conditions are formulated to prevent soft impacts at the start of the zone I in the position  $A$  and at the end of the zone III in the position  $A'$ . This can be achieved by smooth conjugation of the crank radius and its first three derivatives, i.e.

$$\begin{aligned} \lambda_{r4} &= \lambda_{r3} \Big|_{\varphi_1 = \varphi_{1\Sigma}}; \\ \lambda'_{r4} &= \lambda'_{r3} \Big|_{\varphi_1 = \varphi_{1\Sigma}}; \\ \lambda''_{r4} &= \lambda''_{r3} \Big|_{\varphi_1 = \varphi_{1\Sigma}}; \\ \lambda'''_{r4} &= \lambda'''_{r3} \Big|_{\varphi_1 = \varphi_{1\Sigma}} \end{aligned} \quad (13)$$

and

$$\begin{aligned} \lambda_{r4} \Big|_{\varphi_1 = 2\pi} &= \lambda_{r1} \Big|_{\varphi_1 = 0}; \\ \lambda'_{r4} \Big|_{\varphi_1 = 2\pi} &= \lambda'_{r1} \Big|_{\varphi_1 = 0}; \\ \lambda''_{r4} \Big|_{\varphi_1 = 2\pi} &= \lambda''_{r1} \Big|_{\varphi_1 = 0}; \\ \lambda'''_{r4} \Big|_{\varphi_1 = 2\pi} &= \lambda'''_{r1} \Big|_{\varphi_1 = 0} \end{aligned} \quad (14)$$

Since there is infinite number of functions satisfying Eq.(13) and Eq.(14), additional conditions should be formulated. In the bisector of the zone IV, which corresponds to the crank rotation angle  $\varphi_1 = \varphi_c = \varphi_{1\Sigma}/2 + \pi$ , the crank radius  $\lambda_{r4}$  is set equal to the dimensionless limiting radius  $\lambda_{rc}$ , i.e.

$$\lambda_{r4} \Big|_{\varphi_1 = \varphi_c} = \lambda_{rc} \quad (15)$$

and the rate of change of  $\lambda_{r4}$  is set equal to zero, i.e.

$$\lambda'_{r4} \Big|_{\varphi_1 = \varphi_c} = 0 \quad (16)$$



Thereby, the total number of the conditions given by Eqs.(13)–(16) equals  $n = 10$ . These conditions lead to the following system of equations with respect to the coefficients  $a_i$  in Eq.(12):

$$\begin{pmatrix}
 1 & \varphi_{1\Sigma} & \varphi_{1\Sigma}^2 & \varphi_{1\Sigma}^3 & \varphi_{1\Sigma}^4 & \varphi_{1\Sigma}^5 & \varphi_{1\Sigma}^6 & \varphi_{1\Sigma}^7 & \varphi_{1\Sigma}^8 & \varphi_{1\Sigma}^9 \\
 0 & 1 & 2\varphi_{1\Sigma} & 3\varphi_{1\Sigma}^2 & 4\varphi_{1\Sigma}^3 & 5\varphi_{1\Sigma}^4 & 6\varphi_{1\Sigma}^5 & 7\varphi_{1\Sigma}^6 & 8\varphi_{1\Sigma}^7 & 9\varphi_{1\Sigma}^8 \\
 0 & 0 & 2 & 6\varphi_{1\Sigma} & 12\varphi_{1\Sigma}^2 & 20\varphi_{1\Sigma}^3 & 30\varphi_{1\Sigma}^4 & 42\varphi_{1\Sigma}^5 & 56\varphi_{1\Sigma}^6 & 72\varphi_{1\Sigma}^7 \\
 0 & 0 & 0 & 6 & 24\varphi_{1\Sigma} & 60\varphi_{1\Sigma}^2 & 120\varphi_{1\Sigma}^3 & 210\varphi_{1\Sigma}^4 & 336\varphi_{1\Sigma}^5 & 504\varphi_{1\Sigma}^6 \\
 1 & \varphi_e & \varphi_e^2 & \varphi_e^3 & \varphi_e^4 & \varphi_e^5 & \varphi_e^6 & \varphi_e^7 & \varphi_e^8 & \varphi_e^9 \\
 0 & 1 & 2\varphi_e & 3\varphi_e^2 & 4\varphi_e^3 & 5\varphi_e^4 & 6\varphi_e^5 & 7\varphi_e^6 & 8\varphi_e^7 & 9\varphi_e^8 \\
 0 & 0 & 2 & 6\varphi_e & 12\varphi_e^2 & 20\varphi_e^3 & 30\varphi_e^4 & 42\varphi_e^5 & 56\varphi_e^6 & 72\varphi_e^7 \\
 0 & 0 & 0 & 6 & 24\varphi_e & 60\varphi_e^2 & 120\varphi_e^3 & 210\varphi_e^4 & 336\varphi_e^5 & 504\varphi_e^6 \\
 1 & \varphi_c & \varphi_c^2 & \varphi_c^3 & \varphi_c^4 & \varphi_c^5 & \varphi_c^6 & \varphi_c^7 & \varphi_c^8 & \varphi_c^9 \\
 0 & 1 & 2\varphi_c & 3\varphi_c^2 & 4\varphi_c^3 & 5\varphi_c^4 & 6\varphi_c^5 & 7\varphi_c^6 & 8\varphi_c^7 & 9\varphi_c^8
 \end{pmatrix}
 \begin{pmatrix}
 a_1 \\
 a_2 \\
 a_3 \\
 a_4 \\
 a_5 \\
 a_6 \\
 a_7 \\
 a_8 \\
 a_9 \\
 a_{10}
 \end{pmatrix}
 =
 \begin{pmatrix}
 \lambda_{r3} |_{\varphi_{1\Sigma}} \\
 \lambda'_{r3} |_{\varphi_{1\Sigma}} \\
 \lambda''_{r3} |_{\varphi_{1\Sigma}} \\
 \lambda_{r1} |_0 \\
 \lambda'_{r1} |_0 \\
 \lambda''_{r1} |_0 \\
 \lambda_{r1} |_0 \\
 \lambda'_{r1} |_0 \\
 \lambda''_{r1} |_0 \\
 \lambda_{rc} \\
 0
 \end{pmatrix}
 \tag{17}$$

where  $\varphi_e$  stands for  $2\pi$  for shorter notation.

Now it is turn to determine the maximum pressure angle  $\nu_{\max}$  and minimum curvature radius  $\rho_{\min}$  of the cam profile for each zone and compare them to the allowable values  $[\nu]$  and  $[\rho]$ , respectively.

#### 4.1. Limitation condition for the maximum pressure angle

*Zone I.* Substitution of Eq.(11) into Eq.(6) results in the pressure angle  $\nu = \varphi_1$ . Since the crank rotation angle  $\varphi_1$  changes from 0 to  $\Delta\varphi$ , it is true that the maximum pressure angle equals  $\nu_{\max} = \Delta\varphi$ . The condition of Eq.(7) is thus fulfilled if  $\Delta\varphi \leq [\nu]$  or, taking account of Eq.(1) and Eq.(2), if

$$k_{at} \leq \frac{2z}{\pi(z-2)} [\nu]
 \tag{18}$$

Fig.5a shows the range of the additional dwell coefficient  $k_{at}$  that satisfies Eq.(18). The coefficient  $k_{at}$  can take any value between 0 and 0.7 for  $z \in \{3,4\}$ . As the number  $z$  of slots increases, the upper limit of the range decreases. For  $z = 15$ , it equals 0.417 at  $[\nu] = 32.5^\circ$  and 0.532 at  $[\nu] = 41.6^\circ$

[insert Figure 5.]

*Zone II.* Substitution of Eq.(3) and Eq.(4) into Eq.(6) allows deriving the expression of the pressure angle  $\nu$  in the form

$$\tan \nu = \frac{\sin(\varphi_1 + \varphi_2) \sin(\pi/z - \varphi_2) - \varphi_2' \cos(\pi/z + \varphi_1)}{\cos(\varphi_1 + \varphi_2) \sin(\pi/z - \varphi_2)}
 \tag{19}$$

Assume that the wheel moves according to the cycloidal law

$$a_k = k - \frac{\sin(2\pi k)}{2\pi}
 \tag{20}$$

which is widespread in the cyclic mechanisms, providing zero angular acceleration of the wheel in its extreme positions, i.e. at the start and end of its motion period.

The maximum pressure angle  $\nu_{\max}$  is determined based on Eq.(19) and Eq.(20). Fig.5b shows the corresponding range of the coefficient  $k_{at}$  satisfying Eq.(7). As in the case of zone I, the coefficient  $k_{at}$  can be arbitrary from 0 to 0.7 for  $z \in \{3,4\}$ . As the number  $z$  increases, the upper

limit of the range decreases. For  $z = 15$ , it equals 0.375 at  $[\nu] = 32.5^\circ$  and 0.506 at  $[\nu] = 41.6^\circ$ . Comparison of Fig.5a and Fig.5b shows that the coefficient  $k_{at}$  is smaller in the zone II for any  $z$ .

*Zone III.* Since the zones I and III are symmetrical about the vertical axis (see Fig.4), similar conclusions can be drawn here as for the zone I.

*Zone IV.* The crank radius  $\lambda_{r4}$  represents the polynomial of Eq.(12) with the coefficients  $a_i$  satisfying Eq.(17). The dependence of the maximum pressure angle  $\nu_{max}$  on the number  $z$  and limiting radius  $\lambda_{rc}$  is obtained based on Eq.(6). Fig.6 shows the relevant data for the limiting radius  $\lambda_{rc}$  that changes from 1 to 2.2 with step 0.2. It is seen that for  $[\nu] = 32.5^\circ$ , the condition of Eq.(7) is fulfilled at  $1 \leq \lambda_{rc} \leq 2$  and any  $z$ , as well as at  $\lambda_{rc} = 2.2$  and  $z \leq 7$ . For  $[\nu] = 41.6^\circ$ , the entire range of  $\lambda_{rc}$  satisfies the condition of Eq.(7). Note that the maximum pressure angle  $\nu_{max}$  increases with increasing  $\lambda_{rc}$ .

[insert Figure 6.]

Summarising the results for all zones leads to the conclusion that the condition of Eq.(7) limiting the maximum pressure angle  $\nu_{max}$  can be fulfilled for any  $z$ . As the number  $z$  increases, the upper limit of the coefficient  $k_{at}$  decreases. For  $[\nu] = 32.5^\circ$ , it equals 0.7 at  $z = 3$  and 0.375 at  $z = 15$ , whilst for  $[\nu] = 41.6^\circ$ , it is about 1.3 times larger. The coefficient  $k_{at}$  should be chosen according to the results obtained for the zone II (see Fig.5b). Additionally, the limiting radius  $\lambda_{rc}$  should be specified as small as possible to reduce the maximum pressure angle  $\nu_{max}$ .

#### 4.2. Limitation condition of the minimum curvature radius of the cam profile

*Zone I.* Since the path  $AA_1$  of the driving pin is linear (see Fig.4), the curvature radius of the cam profile is infinitely large.

*Zone II.* Substitution of Eq.(20) into Eqs.(3)–(5) allows determining the allowable curvature radius  $[\rho]$  of the cam profile due to Eq.(8) and the minimum curvature radius  $\rho_{min}$  of the cam profile due to Eq.(9). Fig.7 shows the range of the coefficient  $k_{at}$  satisfying the condition of Eq.(10) in dependence on the number  $z$ . The analysis reveals that for  $[\nu] = 32.5^\circ$ , the synthesis of the driving pin path is possible at  $z \geq 4$ . The coefficient  $k_{at}$  is in range from 0 to 0.29 at  $4 \leq z \leq 13$  and in range from 0 to 0.28 at  $z \in \{14,15\}$ . As for  $[\nu] = 41.6^\circ$ , the condition of Eq.(10) is fulfilled for any  $z$ . The upper limit of the coefficient  $k_{at}$  equals 0.34 at  $z = 3$ , 0.37 at  $z \in \{4,5,6,13,14,15\}$  and 0.38 at  $7 \leq z \leq 12$ .

[insert Figure 7.]

*Zone III.* Similar conclusions are valid as for the zone I due to the symmetry of the zones I and III about the vertical axis (see Fig.4).

*Zone IV.* The crank radius  $\lambda_{r4}$  is described by the polynomial Eq.(12) with the coefficients  $a_i$  satisfying Eq.(17). Fig.8 shows the allowable curvature radius  $[\rho]$  of the cam profile determined based on Eq.(8). Fig.9 shows the minimum curvature radius  $\rho_{min}$  of the cam profile determined by Eq.(9).

[insert Figure 8.]

[insert Figure 9.]

Fig.8 and Fig.9 suggest that the condition of Eq.(10) is fulfilled almost in the entire ranges of the number  $z$  and limiting radius  $\lambda_{rc}$ . For  $[\nu] = 32.5^\circ$  and  $\lambda_{rc} = 2.2$ , this condition is fulfilled at  $z$



1  
2  
3  $\leq 10$ . The limiting radius  $\lambda_{rc}$  should take the smallest possible value to reduce the geometric  
4 dimensions of the mechanism whilst providing a single-sign curvature path of the driving pin.

5 Thereby, Figs.5–9 outline the set of the groove cam Geneva mechanisms that provide the  
6 double locking of the wheel at its dwell-to-motion and motion-to-dwell transitions, absence of soft  
7 impacts in the extreme positions and significantly wider range of the operating time coefficient  $k_w$   
8 compared to the conventional Geneva mechanisms. It should be noted that the developed method is  
9 not limited by the type of function given by Eq.(20) and can be applied for arbitrary law of motion  
10 of the wheel.  
11

## 12 5. Synthesis algorithm

13 The theoretical results obtained in Sections 2–4 can be combined into one algorithm  
14 presented in Fig.10. At the first stage, the number  $z$  of slots and the operating time coefficient  $k_w$   
15 are determined by Eq.(2). At the second stage, the cam profile is checked for the maximum pressure  
16 angle  $\nu_{max}$  due to Eq.(7). As mentioned in Section 4.1, the symmetry of the cam profile in the zones  
17 I and III should be taken into consideration. At the third stage, the cam profile is checked for the  
18 minimum curvature radius  $\rho_{min}$  due to Eq.(10). Remind that the check is not performed for the  
19 zones I and III where the driving pin path is linear. If at least one of the conditions Eq.(7) and  
20 Eq.(10) is not fulfilled, the algorithm returns to the first stage.  
21

22 Repetition of the first three stages leads to the fourth stage which consists in forming the set  
23 of pairs  $z$  and  $k_w$  that satisfy the main and additional conditions of synthesis. The fifth stage is  
24 selection of the optimum solution. In general, a smaller value of  $k_w$  corresponds to a higher  
25 productivity of the machine employing the groove cam Geneva mechanism but also to higher  
26 inertial loads on the mechanism. Therefore, a dynamic analysis of the mechanism considering  
27 inertial masses attached to the wheel is necessary to evaluate the margin of strength that can be  
28 sacrificed in favour of productivity. At the sixth stage, the cam profile is drawn based on the  
29 synthesised path of the driving pin.  
30

31 Since in the present study the centre  $C$  of the roller follower 5 is assumed to coincide with  
32 the centre  $A$  of the driving pin 4 (see Fig.2), i.e. the cam profile is identical to the path of the centre  
33  $A$ , the final stage of the algorithm does not require calculations. In the general case, this assumption  
34 is not true, and the cam profile is to be drawn based on the path of the driving pin centre  $A$ .  
35 Obviously, the expressions derived in Sections 3 and 4 become more cumbersome in this case.  
36 Nonetheless, the general approach presented in Section 2 and summarised by the algorithm in  
37 Fig.10 remains valid.  
38

39  
40  
41  
42 [insert Figure 10.]  
43  
44

## 45 6. Method application

46 For example, consider a problem of synthesising the Geneva mechanism with operating time  
47 coefficient  $k_w = 0.3$ . Fig.3 shows that none of the number  $z$  of slots satisfies  $k_w = 0.3$  and  $k_{at} = 0$ ,  
48 i.e. the conventional Geneva mechanism cannot provide the required value of  $k_w$ . Find the solution  
49 using the algorithm proposed in Fig.10, accepting the allowable pressure angle equal to  $[\nu] = 41.6^\circ$ .

50 Table 1 presents the pairs  $z$  and  $k_{at}$  that provide  $k_w = 0.3$  due to Eq.(2). The set of solutions  
51 is thus  $4 \leq z \leq 15$ . Fig.5 and Fig.6 show that the condition of Eq.(7) is fulfilled in the zones I–IV  
52 for any values of  $z$  in the entire range of the limiting radius  $\lambda_{rc}$ , i.e. this condition does not narrow  
53 down the set of solutions. On the other hand, due to Fig.7, the condition of Eq.(10) is fulfilled in the  
54 zone II at  $z \leq 7$ . Comparison of Fig.8 and Fig.9 suggests no additional limitations in the zone IV.  
55 Thereby, the set of solutions is narrowed down by Eq.(10) to  $4 \leq z \leq 7$ . Fig.11a presents the  
56 synthesised paths of the driving pin for the limit values of  $z$  at  $\lambda_{rc} = 1$ . The solution  $z = 4$  provides  
57 minimum inertia load on the mechanism, whereas the solution  $z = 7$  maximises the machine  
58 productivity.  
59  
60



Table 1. Pairs of the number  $z$  of slots and additional dwell coefficient  $k_{at}$  providing  $k_w = 0.3$ 

$z$	4	5	6	7	8	9	10	11	12	13	14	15
$k_{at}$	0.0769	0.231	0.308	0.354	0.385	0.407	0.423	0.436	0.446	0.456	0.462	0.468

Now consider another problem that consists in synthesising the Geneva mechanism with specified number of slots  $z = 8$ . For the sake of variety, the allowable pressure angle is set equal to  $[\nu] = 32.5^\circ$  in this example.

Fig.3 outlines the infinite set of solutions for  $z = 8$  in the form of  $k_{at}$  ranging between 0 to 0.7. The check of Eq.(7) shows that  $k_{at}$  is limited from above by 0.48 in the zones I and III, as shown in Fig.5a, and by 0.46 in the zone II, as shown in Fig.5b. Due to Fig.6 for the zone IV, the limiting radius  $\lambda_{rc}$  may vary between 1 and 2. Further, the check of Eq.(10) shows that  $k_{at}$  is limited from above by 0.29 in the zone II, as shown in Fig.7, whilst there are no additional limitations in the zone IV, as shown in Fig.8 and Fig.9. The set of solutions is thereby limited by Eq.(7) and Eq.(10) to the range  $0 \leq k_{at} \leq 0.29$ . Fig.11b shows the synthesised paths of the driving pin for the limit values of  $k_{at}$  at  $\lambda_{rc} = 1$ . The solution  $k_{at} = 0$  has the same operating time coefficient  $k_w = 0.6$  as the conventional Geneva mechanism. In contrast, the solution  $k_{at} = 0.29$  corresponds to  $k_w = 0.37$ , i.e. the groove cam Geneva mechanism synthesised by the algorithm in Fig.10 allows improving the machine productivity by  $(1 + 0.6)/(1 + 0.37) \approx 1.17$  times.

[insert Figure 11.]

## 7. Conclusions

A synthesis method for the groove cam external Geneva mechanisms with increased dwell period is developed which provides the required law of motion of the wheel with account of the conditions limiting the maximum pressure angle  $\nu_{max}$  and minimum curvature radius  $\rho_{min}$  of the cam profile.

It is shown that unlike the conventional Geneva mechanisms, the synthesised groove cam Geneva mechanisms enable:

- arbitrary law of motion of the wheel;
- double locking of the wheel at its dwell-to-motion and motion-to-dwell transitions;
- absence of soft impacts in the extreme positions;
- significantly wider range of the operating time coefficient  $k_w$ .

The dimensionless analysis performed for the cycloidal law of motion, number  $z$  of slots in range from 3 to 15, additional dwell coefficient  $k_{at}$  in range from 0 to 0.7 shows that the operating time coefficient  $k_w$  is provided in range from 0.053 to 0.765. The advantages of the synthesised groove cam Geneva mechanisms over the conventional Geneva mechanisms are clearly illustrated by the numerical examples.

## Declaration of conflicting interests

The authors declare that there is no conflict of interest.

## Funding

The authors received no financial support for the research, authorship, and/or publication of this article.

## References

1. Bickford JH. *Mechanisms for intermittent motion*. New York: Industrial Press Inc., 1972, pp.127–138.

2. Chironis NP, Nicholas P. *Mechanisms and mechanical devices sourcebook*. New York: McGraw-Hill, 1991.
3. Prajapati A, Patel C, Pankhania D, et al. Review on Geneva mechanism and its application. *Int J Adv Eng Res Dev* 2017; 4 (2): 425–429.
4. Beltz RK, Hurst JC. Peristaltic pump metering and dispensing system. *Technical Digest - Western Electric Company*, 1975, no.37, pp.3–4.
5. Pazouki ME, Jones JR. The kinematic synthesis of a linkage driven Geneva mechanism. *Mech Mach Theory* 1982; 17 (3): 221–228.
6. Meyer G. A tested method for precise intermittent motion. *Mach Des* 1988; 60 (1): 140–143.
7. Egorov OD, Nadezhdin IV. Use of Geneva mechanisms in industrial robots. *Sov Eng Res* 1988; 8 (11): 134–137.
8. Lee JJ, Cho CC. Improving kinematic and structural performance of Geneva mechanism using the optimal control method. *Proc Inst Mech Eng C J Mech Eng Sci* 2002; 216 (7): 761–774.
9. Kali Sindhur P, Karthik Y, vijay T, et al. Cutting mechanism by giving through Geneva mechanism. *Int J Innov Sci Eng Technol* 2015; 2 (4): 1172–1175.
10. Ujam AJ, Ejeogo G, Onyeneho KC. Development and application of Geneva mechanism for bottle washing. *Am J Eng Res* 2015; 4 (11): 63–73.
11. Zhang E, Wang L. Parametric design and motion analysis of Geneva wheel mechanism based on the UG NX8.5. In: *International Conference on Manufacturing Engineering and Intelligent Materials*, Advances in Engineering, 2017, vol.100, pp.352–356.
12. Sepahpour B. *Kinematic and kinetic analysis of Geneva mechanisms and their applications to synchronization of motion*. PhD Thesis, New Jersey Institute of Technology, 1994.
13. Figliolini G, Rea P, Angeles J. The pure-rolling cam-equivalent of the Geneva mechanism. *Mech Mach Theory* 2006; 41 (11): 1320–1335.
14. Shaohua S, Jifei C. Kinematic analysis on series combined mechanism of elliptic gear and outer Geneva. *Appl Mech Mater* 2013; 312: 42–46.
15. Dijkstra EA. Jerk-free Geneva wheel driving. *J Mech* 1966; 1 (3–4): 235–280.
16. Bagci C. Synthesis of double-crank driven mechanisms with adjustable motion and dwell time ratios. *Mech Mach Theory* 1977; 12 (6): 619–638.
17. Yang AT, Hsia LM. Multistage geared Geneva mechanism. *Trans ASME J Mech Des* 1979; 101 (1): 41–46.
18. Fenton RG. Geneva mechanisms connected in series. *Trans ASME J Manuf Sci Eng* 1975; 97: 603–608.
19. Al-Sabeeh AK. Double crank external Geneva mechanism. *Trans ASME J Mech Des* 1993; 115: 666–670.
20. Figliolini G, Rea P. Effects of the design parameters on the synthesis of Geneva mechanisms. *Proc Inst Mech Eng C J Mech Eng Sci* 2012; 227 (9): 2000–2009.
21. Yang AT, Hsia LM. Multistage geared Geneva mechanism. *Trans ASME J Mech Des* 1979; 101: 41–46.
22. Sujana VA, Meggiolaro MA. Dynamic optimization of Geneva mechanisms. In: *International Conference on Gearing, Transmissions and Mechanical Systems*, 2000, pp.687–696.
23. Sadek KSH., Lloyd JL, Smith MR. A new design of Geneva drive to reduce shock loading. *Mech Mach Theory* 1990; 25: 589–595.
24. Cheng CY, Lin Y. Improving dynamic performance of the Geneva mechanism using non-linear spring elements. *Mech Mach Theory* 1995; 30: 119–129.
25. Fenton RG, Zhang Y, Xu J. Development of a new Geneva mechanism with improved kinematic characteristics. *Trans ASME J Mech Des* 1991; 113 (1): 40–45.
26. Lee HP. Design of a Geneva mechanism with curved slots using parametric polynomials. *Mech Mach Theory* 1998; 33 (3): 321–329.
27. Lee JJ, Huang KF. Geometry analysis and optimal design of Geneva mechanisms with curved slots. *Proc Inst Mech Eng C J Mech Eng Sci* 2004; 218 (4): 449–458.

28. Lee JJ, Jan BH. Design of Geneva mechanisms with curved slots for non-undercutting manufacturing. *Mech Mach Theory* 2009; 44 (6): 1192–1200.
29. Li HT. Design of a new kind of curved groove on Geneva mechanism. *J China Agric Univ* 2005; 10: 62–65.
30. DuMont CL, Kurtz AF, Silverstein BD, et al. Design improvement for motion picture film projectors. In: *143rd Technical Conference and Exhibition*, New York, 2001, pp.785–791.
31. Zhang J, Sun S, Tuan HA. Optimization design and analysis of rotary indexing mechanism of tool magazine in machining center. *Jordan J Mech Ind Eng* 2020; 14 (1): 1–6.
32. Heidari M, Atai AA, Shariat Panahi M. An improved Geneva mechanism for optimal kinematic performance. *Proc Inst Mech Eng C J Mech Eng Sci* 2012; 226 (6): 1515–1525.
33. Polyudov OM. *Mechanics of printing machines*. Kyiv: NMKVO, 1991.
34. Uicker JJ, Pennock GR, Shigley JE. *Theory of machines and mechanisms*. 5th ed. New York: Oxford University Press, 2017.

For Peer Review

## A method to synthesise groove cam Geneva mechanisms with increased dwell period

Viacheslav Pasika<sup>a</sup>, Pavlo Nosko<sup>b</sup>, Oleksii Nosko<sup>c\*</sup>, Oleksandr Bashta<sup>b</sup>, Volodymyr Heletiy<sup>a</sup>,  
Volodymyr Melnyk<sup>b</sup>

<sup>a</sup>Lviv Polytechnic National University,  
Department of Technical Mechanics and Dynamics of Machines, Bandery 32, Lviv, 79013, Ukraine

<sup>b</sup>National Aviation University, Aerospace Faculty, Department of Applied Mechanics and  
Materials Engineering, Lubomyr Husar 1, Kyiv, 03058, Ukraine

<sup>c</sup>Gdansk University of Technology, Faculty of Mechanical Engineering and Ship Technology,  
Narutowicza 11/12, Gdansk, 80233, Poland

\*Corresponding author: [oleksii.nosko@pg.edu.pl](mailto:oleksii.nosko@pg.edu.pl), <https://orcid.org/0000-0002-5259-1426>

### Abstract

The present study develops a method to synthesise the groove cam Geneva mechanism with increased dwell period. The main condition of the synthesis is to provide the desired law of motion of the wheel. Additional synthesis conditions are the limitation of the maximum pressure angle and the limitation of the minimum curvature radius of the cam profile. Unlike the conventional Geneva mechanisms, the synthesised groove cam Geneva mechanisms enable motion of the wheel due to an arbitrarily specified law, double locking of the wheel at its dwell-to-motion and motion-to-dwell transitions, absence of soft impacts in the extreme positions. The analysis shows that for the cycloidal law of motion, number of slots in range 3 to 15 and additional dwell coefficient in range 0 to 0.7, the operating time coefficient can be provided in wide range from 0.053 to 0.765. The effectiveness of the method is illustrated by numerical examples.

Keywords: Geneva mechanism, groove cam Geneva mechanism, synthesis method, number of wheel slots, operating time coefficient, additional dwell coefficient

## Notation

$a_k$	wheel rotation invariant
$b_k$	wheel angular velocity invariant
$c_k$	wheel angular acceleration invariant
$k$	dimensionless time
$k_{at}$	additional dwell coefficient
$k_w$	operating time coefficient
$l_{AB}$	distance between the wheel axis and driving pin axis
$l_{OA}$	initial crank radius
$l_{OB}$	distance between the crank rotation axis and wheel axis
$r$	crank radius
$t_s$	wheel dwell period
$t_t$	wheel motion period
$z$	number of slots
$\lambda_2$	dimensionless distance between the wheel axis and driving pin axis
$\lambda_a$	dimensionless distance between the crank rotation axis and wheel axis
$\lambda_r$	dimensionless crank radius
$\lambda_{r1, \dots, \lambda_{r4}}$	dimensionless crank radius in the zones I, ..., IV
$\lambda_{rc}$	dimensionless limiting radius
$\nu$	pressure angle
$\nu_{max}$	maximum pressure angle
$[\nu]$	allowable pressure angle
$\rho_{min}$	dimensionless minimum curvature radius of the cam profile
$[\rho]$	dimensionless allowable curvature radius of the cam profile
$\varphi_1$	crank rotation angle
$\varphi_2$	wheel rotation angle
$\varphi_{1\Sigma}$	total crank rotation angle
$\varphi_{2\Sigma}$	total wheel rotation angle
$\omega_1$	crank angular velocity
$\omega_2$	wheel angular velocity
$\Delta\varphi$	additional dwell angle



## 1. Introduction

Increasing speeds and productivity of automatic machines require employment of highly functional and efficient cyclic mechanisms. Geneva mechanisms belong to the cyclic mechanisms commonly used in automatic machines [1–3]. Their application range is extensive and has evolved from mechanical watches and motion-picture projectors to discrete motion drives in robotic manipulators and CNC machines [4–10].

The Geneva mechanisms are simple, technological and undemanding in maintenance. However, like all lever mechanisms, they possess certain disadvantages. First of all, the laws of motion of the wheel are characterised by impact phenomena in its extreme positions, which imposes speed and energy limitations. Moreover, in the Geneva mechanism with a constant crank radius and a fixed number  $z$  of slots on the wheel, the operating time coefficient  $k_w = t_t/t_s$  equal to the ratio of the motion period  $t_t$  of the wheel to its dwell period  $t_s$  is governed by the number  $z$  as per the equality  $k_w = (z - 2)/(z + 2)$ . Adjusting the coefficient  $k_w$  by changing the number  $z$  is not feasible in many practical cases [11].

There is a class of automatic machines and automated lines employing the Geneva mechanism where most technological operations are performed when the wheel is stationary. This class includes but is not limited to engine lathe machines, carousel lathe machines, cutting machines, milling machines, drilling machines, packaging machines, conveyor machines, lining machines. For example, if the Geneva mechanism is used in a bottle filling machine, rotation of the wheel provides placing the consecutive empty bottle under the valve, whilst filling of the bottle with liquid takes place during the dwell period  $t_s$ . The productivity of such automatic machines can be thus improved by reducing the motion period  $t_t$  or, in other words, increasing the dwell period  $t_s$ . However, if large inertial masses are attached to the wheel, the motion period  $t_t$  cannot be reduced without a significant increase in the wheel angular acceleration and, accordingly, inertial loads.

Further, the disadvantages of the Geneva mechanisms include the fact that the wheel is locked solely by a locking ring [12]. As the driving pin of the crank enters the slot, the edge of the locking ring, which is rigidly connected to the crank, comes out of contact with the wheel. High accuracy should be, therefore, guaranteed for the mutual location between the crank and locking ring. Errors in the manufacture and installation of the mechanism and its wear lead to the occurrence of unwanted gaps. This, in its turn, results in non-simultaneous entry of the driving pin into the slot and exit of the locking ring from contact, which is accompanied by increased impact loads. A similar situation is observed when the driving pin leaves the slot.

Several approaches have been proposed to improve the dynamic performance of the Geneva mechanisms. The first approach implies application of compound mechanisms to eliminate soft impacts (discontinuous accelerations) in the extreme positions [13–22]. Two or more mechanisms are connected in series so that the angular acceleration of the wheel changes continuously during its motion. This approach inevitably introduces extra components to the system. The second approach is using damping elements in the Geneva mechanism in order to reduce the impact loads [23, 24], which also leads to extra components in the system. The third approach is to modify the geometry of the slots [25–29]. Curvilinear slots are designed to provide the desired law of motion, similarly as in cam mechanisms. Although processing of the curvilinear slots is resource consuming, the approach enables adjusting the dwell period  $t_s$  even for a fixed number  $z$  of slots.

The study [30] investigates the applicability of the wheel with barrel-shaped slots, called ‘Quickermittent’, for motion picture film projectors. Such a mechanism allows to reduce the indexing time whilst maintaining control over the loads on the film and mechanism itself. However, due to the fact that the slot is wider in its middle part, the driving pin can hit the walls of the slot, which affects adversely on the motion stability, especially at low rotational speeds. In addition, Quickermittent mechanisms tend to be noisier than the Geneva mechanisms.

A double-pins without locking arc Geneva mechanism is developed in the study [31]. The proposed mechanism has two driving pins in contrast to the conventional Geneva mechanism with one driving pin, resulting in two times higher angular velocity of the wheel. Smaller impact loads in

the mechanism are achieved by optimising the transitional part of the slot, which implies, however, higher manufacturing costs.

The studies [2, 8, 32, 33] suggest that the functionality of the Geneva mechanism can be substantially extended by introducing a groove cam element. The groove cam Geneva mechanism comprises input crank 1, output wheel 2, groove cam 3, driving pin 4 and roller follower 5, as shown in Fig.1. The crank 1 rotates at constant angular velocity  $\omega_1$  and simultaneously moves radially due to the path of the roller follower 5 along the groove of the cam 3. The driving pin 4 on the crank 1 brings the wheel 2 in motion. Thus, the mechanism makes use of the cam 3 to control the radius of action of the driving pin 4, which provides the necessary kinematic characteristics of the wheel 2.

[insert Figure 1.]

The analysis of the above-mentioned studies indicates a lack of research devoted to solving the problem of synthesising the groove cam Geneva mechanism and analysing the influence of different parameters on its performance. The purpose of the present study is to develop a method to synthesise the groove cam Geneva mechanism with increased dwell period that satisfies the desired law of motion of the wheel (main condition), allowable pressure angle and allowable curvature radius of the cam profile (additional conditions). The following tasks are solved to achieve this purpose: development of the general approach to determining the path of the driving pin due to the specified operating time coefficient  $k_w$  (Section 2); formulation of the additional conditions of synthesis (Section 3); development of the method to synthesise the driving pin path (Section 4); development of the synthesis algorithm (Section 5); illustration of the method application (Section 6).

## 2. General approach to determining the driving pin path

A detailed schematic of the groove cam Geneva mechanism is shown in Fig.2. The numbering of the elements in the schematic corresponds to Fig.1. In addition to the input crank 1, output wheel 2, groove cam 3, driving pin 4 and roller follower 5, Fig.2 presents the locking ring 6. To reduce the number of parameters in the present study and simplify analysis, the roller follower 5 is assumed to have a common axis with the driving pin 4, i.e. the centre  $C$  of the roller follower 5 coincides with the centre  $A$  of the driving pin 4. Under this assumption, the profile of the cam 3 coincides with the path of the centre  $A$  of the driving pin 4.

[insert Figure 2.]

Imagine that the driving pin 4 enters the slot of the wheel 2 at the moment when the crank 1 and slot are mutually perpendicular. The driving pin 4 passes then along the slot from the position  $A$  to the position  $A_1$ , which corresponds to a certain rotation angle  $\Delta\varphi$  of the crank 1. In this interval, the wheel 2 is stationary due to its locking by the ring 6 and motion of the driving pin 4 along the line  $AA_1$ . As the crank 1 rotates by the angle  $\Delta\varphi$ , the wheel 2 is brought in motion. Apparently, the described situation corresponds to an increase in the dwell period  $t_s$  of the wheel 2. The angle  $\Delta\varphi$  is referred to as ‘additional dwell angle’.

There is thus a principal difference between the operation of the conventional Geneva mechanism and that of the groove cam Geneva mechanism. In the former, the locking of the wheel at its dwell-to-motion and motion-to-dwell transitions is performed solely by the locking ring, whereas in the latter it is performed by both locking ring 6 and driving pin 4.

Derive an analytical expression for the operating time coefficient  $k_w$ . Introduce the total crank rotation angle  $\varphi_{1\Sigma}$  and total wheel rotation angle  $\varphi_{2\Sigma}$  as

5

$$\varphi_{1\Sigma} = \pi \left( 1 - \frac{2}{z} \right);$$

$$\varphi_{2\Sigma} = \frac{2\pi}{z}$$

Further, express the motion period  $t_t$  and dwell period  $t_s$  in the form

$$t_t = \frac{\varphi_{1\Sigma} - 2\Delta\varphi}{\omega_1};$$

$$t_s = \frac{2\pi - \varphi_{1\Sigma} + 2\Delta\varphi}{\omega_1}$$

Based on the equations above, the operating time coefficient  $k_w$  can be expressed as follows:

$$k_w = \frac{t_t}{t_s} = \frac{\pi(z-2)/z - 2\Delta\varphi}{\pi(z+2)/z + 2\Delta\varphi} \quad (1)$$

After defining the additional dwell coefficient as the ratio

$$k_{at} = \frac{2\Delta\varphi}{\varphi_{1\Sigma}}$$

Eq.(1) can be rewritten in the following manner:

$$k_w = \frac{(z-2)(1-k_{at})}{2z - (z-2)(1-k_{at})} \quad (2)$$

Apparently, the operating time coefficient  $k_w$  is reduced at  $\Delta\varphi > 0$  and, accordingly,  $k_{at} > 0$ . As the coefficient  $k_{at}$  tends to 1, the additional dwell angle  $\Delta\varphi$  increases significantly along with the geometric dimensions of the mechanism (see Fig.2). It is reasonable, therefore, to limit  $k_{at}$ , and the present study accepts that  $k_{at} \leq 0.7$ . Due to the fact that the number  $z$  of slots cannot be less than 3, whilst the Geneva mechanisms with  $z > 15$  are rarely met in practice, the number  $z$  is accepted to be in range from 3 to 15.

Fig.3 illustrates the dependence of the operating time coefficient  $k_w$  on the additional dwell coefficient  $k_{at}$  and number  $z$  due to Eq.(2). The analysis shows that for the conventional Geneva mechanism ( $k_{at} = 0$ ), the coefficient  $k_w$  changes from 0.2 to 0.765. By contrast, the groove cam Geneva mechanism has a significantly wider range of the coefficient  $k_w$  from 0.053 to 0.765 at  $0 < k_{at} \leq 0.7$ . Note that the coefficient  $k_w$  is more sensitive to the variation of  $k_{at}$  at smaller values of  $k_{at}$ .

[insert Figure 3.]

Considering Fig.2, introduce the dimensionless crank radius  $\lambda_r$ , dimensionless distance  $\lambda_2$  between the driving pin axis  $A$  and wheel axis  $B$ , dimensionless distance  $\lambda_a$  between the crank rotation axis  $O$  and wheel axis  $B$  as

$$\lambda_r = \frac{r}{l_{OA}};$$

$$\lambda_2 = \frac{l_{AB}}{l_{OA}};$$

$$\lambda_a = \frac{l_{OB}}{l_{OA}} = \frac{1}{\sin(\pi/z)}$$



where  $r$  is the crank radius, i.e. the distance between the crank rotation axis  $O$  and driving pin axis  $A$ ;  $l_{AB}$  is the distance between the driving pin axis  $A$  and wheel axis  $B$ ;  $l_{OB}$  is the distance between the crank rotation axis  $O$  and wheel axis  $B$ ;  $l_{OA}$  is the initial crank radius for the perpendicular position between the crank and slot.

Writing the equation of closed vector circuit in the form

$$\bar{\lambda}_r + \bar{\lambda}_2 = \bar{\lambda}_a$$

and projecting it on the horizontal and vertical axes yield that

$$\lambda_r = \lambda_a \frac{\sin(\pi/z - \varphi_2)}{\cos(\varphi_1 + \varphi_2)};$$

$$\lambda_2 = \lambda_a \frac{\cos(\pi/z + \varphi_1)}{\cos(\varphi_1 + \varphi_2)}$$

(3)

where  $\varphi_1$  and  $\varphi_2$  are the rotation angles of the respective crank and wheel.

Further, represent the rotation angles of the respective crank and wheel in the form

$$\varphi_1 = k\varphi_{1\Sigma};$$

$$\varphi_2 = a_k\varphi_{2\Sigma}$$

where  $k = \varphi_1/\varphi_{1\Sigma}$  is the dimensionless time;  $a_k$  is the wheel rotation invariant. Then the derivatives of the radius  $\lambda_r$  with respect to  $\varphi_1$  read

$$\lambda'_r = \frac{d\lambda_r}{d\varphi_1} = \frac{\lambda_a}{\cos^2(\varphi_1 + \varphi_2)} \left( \sin(\varphi_1 + \varphi_2) \sin\left(\frac{\pi}{z} - \varphi_2\right) - \varphi'_2 \cos\left(\frac{\pi}{z} + \varphi_1\right) \right);$$

$$\lambda''_r$$

$$= \frac{d^2\lambda_r}{d\varphi_1^2} = -\frac{\lambda_a}{\cos^3(\varphi_1 + \varphi_2)} \left( \varphi''_2 \cos(\varphi_1 + \varphi_2) \cos\left(\frac{\pi}{z} + \varphi_1\right) + 2\varphi'_2 \left( (1 + \varphi'_2) \cos(\varphi_1 + \varphi_2) \sin\left(\frac{\pi}{z} + \varphi_1\right) - (2 + \varphi'_2) \sin\left(\frac{\pi}{z} - \varphi_2\right) \right) + (1 + \sin^2(\varphi_1 + \varphi_2)) \sin\left(\frac{\pi}{z} - \varphi_2\right) \right)$$

(4)

with

$$\varphi'_2 = \frac{d\varphi_2}{d\varphi_1} = b_k \frac{\varphi_{2\Sigma}}{\varphi_{1\Sigma}};$$

$$\varphi''_2 = \frac{d^2\varphi_2}{d\varphi_1^2} = c_k \frac{\varphi_{2\Sigma}}{\varphi_{1\Sigma}^2}$$

(5)

where  $b_k = da_k/dk$  and  $c_k = db_k/dk$  are the wheel angular velocity and acceleration invariants.

Thus, as the crank radius  $\lambda_r$  changes due to Eq.(3), the wheel moves according to the prescribed law with rotation invariant  $a_k$ . Remember that the expressions for  $\lambda_r$ ,  $\lambda'_r$ ,  $\lambda''_r$  given by Eqs.(3)–(5) are valid if the wheel motion starts from the perpendicular position between the crank and slot.

### 3. Additional conditions of synthesis

Since the studied mechanism (see Fig.2) includes a cam mechanism in the form of the roller follower in contact with the groove cam, the additional conditions of synthesis arise, as considered next.

### 3.1. Limitation condition for the maximum pressure angle

In order to prevent jamming in the cam mechanism, the maximum value  $\nu_{\max}$  of the pressure angle

$$\nu = \arctan \frac{\lambda'_r}{\lambda_r} \quad (6)$$

should not exceed the allowable pressure angle  $[\nu]$ . The corresponding condition limiting the maximum pressure angle  $\nu_{\max}$  is formulated as

$$\nu_{\max} \leq [\nu] \quad (7)$$

The allowable pressure angle  $[\nu]$  is chosen depending on the angular velocity and load in the cam mechanism. In most engineering applications, the value of  $[\nu]$  is in range from  $30^\circ$  to  $45^\circ$ . In the present study,  $[\nu]$  is accepted to be between  $32.5^\circ$  and  $41.6^\circ$ , which corresponds to the case of rotary tables like Vertex Precision Tilting Rotary Table VUT used in carousel lathe machines, cutting machines, milling machines, drilling machines and conveyor machines [33].

### 3.2. Limitation condition for the minimum curvature radius of the cam profile

In order to prevent sharpening and interference of the cam profile, it is necessary to limit from below its minimum curvature radius  $\rho_{\min}$ . The allowable curvature radius  $[\rho]$  of the cam profile is determined by the dimensionless expression [34]

$$[\rho] = \max \left\{ \frac{\lambda'_r}{\tan [\nu]} - \lambda_r + \min \lambda_r \right\} \quad (8)$$

The minimum curvature radius  $\rho_{\min}$  of the cam profile is derived from the known formula for the radius of curvature given in polar coordinates as

$$\rho_{\min} = \min \left\{ \frac{(\lambda_r^2 + (\lambda'_r)^2)^{3/2}}{\lambda_r^2 + 2(\lambda'_r)^2 - \lambda_r \lambda''_r} \right\} \quad (9)$$

The condition limiting the minimum curvature radius  $\rho_{\min}$  takes then the following form:

$$\rho_{\min} \geq [\rho] \quad (10)$$

Thus, the additional conditions of synthesis include Eq.(7) limiting the maximum pressure angle  $\nu_{\max}$  and Eq.(10) limiting the minimum curvature radius  $\rho_{\min}$  of the cam profile.

## 4. Method to synthesise the driving pin path

Fig.4 shows the characteristic zones of the crank motion: I — linear path of the driving pin, stationary wheel; II — path of the driving pin for the wheel motion period; III — linear path of the driving pin, stationary wheel; IV — path of the driving pin which provides a smooth conjugation of the end of the zone III and the start of the zone I. The crank radius  $\lambda_r$  is determined next for each zone.

[insert Figure 4.]

*Zone I* starts in the position *A* when the driving pin enters the slot, and it ends in the position  $A_1$  when the crank rotates by the additional dwell angle  $\Delta\varphi$ . The rotation angle  $\varphi_1$  of the crank

changes, thereby, from 0 to  $\Delta\varphi$ . Considering the fact that the wheel is stationary, i.e.  $\varphi_2 = 0$ , a simplified expression for the crank radius  $\lambda_{r1}$  is derived in the form

$$\lambda_{r1} = \frac{1}{\cos \varphi_1} \quad (11)$$

*Zone II* starts in the position  $A_1$  and ends in the position  $A'_1$ . The wheel moves according to the prescribed law. The crank rotation angle  $\varphi_1$  changes from  $\Delta\varphi$  to  $(\varphi_{1\Sigma} - \Delta\varphi)$ . The crank radius  $\lambda_{r2}$  is found from Eqs.(3)–(5).

*Zone III* starts in the position  $A'_1$  and ends in the position  $A'$ . The motion of the driving pin occurs similarly to that in the zone I. The crank rotation angle  $\varphi_1$  changes from  $(\varphi_{1\Sigma} - \Delta\varphi)$  to  $\varphi_{1\Sigma}$ . Since  $\varphi_2 = \varphi_{2\Sigma} = 2\pi/z$ , the expression for the crank radius  $\lambda_{r3}$  reads

$$\lambda_{r3} = -\frac{1}{\cos(2\pi/z + \varphi_1)}$$

*Zone IV* starts in the position  $A'$  and ends in the position  $A$ . Accordingly, the crank rotation angle  $\varphi_1$  changes from  $\varphi_{1\Sigma}$  to  $2\pi$ . The crank radius  $\lambda_{r4}$  can be defined in the form of polynomial

$$\lambda_{r4} = \sum_{i=1}^n a_i \varphi_1^{i-1} \quad (12)$$

where  $n$  is the number of the conditions imposed on the crank radius  $\lambda_{r4}$ .

The boundary conditions are formulated to prevent soft impacts at the start of the zone I in the position  $A$  and at the end of the zone III in the position  $A'$ . This can be achieved by smooth conjugation of the crank radius and its first three derivatives, i.e.

$$\begin{aligned} \lambda_{r4} &= \lambda_{r3} \Big|_{\varphi_1 = \varphi_{1\Sigma}}; \\ \lambda'_{r4} &= \lambda'_{r3} \Big|_{\varphi_1 = \varphi_{1\Sigma}}; \\ \lambda''_{r4} &= \lambda''_{r3} \Big|_{\varphi_1 = \varphi_{1\Sigma}}; \\ \lambda'''_{r4} &= \lambda'''_{r3} \Big|_{\varphi_1 = \varphi_{1\Sigma}} \end{aligned} \quad (13)$$

and

$$\begin{aligned} \lambda_{r4} \Big|_{\varphi_1 = 2\pi} &= \lambda_{r1} \Big|_{\varphi_1 = 0}; \\ \lambda'_{r4} \Big|_{\varphi_1 = 2\pi} &= \lambda'_{r1} \Big|_{\varphi_1 = 0}; \\ \lambda''_{r4} \Big|_{\varphi_1 = 2\pi} &= \lambda''_{r1} \Big|_{\varphi_1 = 0}; \\ \lambda'''_{r4} \Big|_{\varphi_1 = 2\pi} &= \lambda'''_{r1} \Big|_{\varphi_1 = 0} \end{aligned} \quad (14)$$

Since there is infinite number of functions satisfying Eq.(13) and Eq.(14), additional conditions should be formulated. In the bisector of the zone IV, which corresponds to the crank rotation angle  $\varphi_1 = \varphi_c = \varphi_{1\Sigma}/2 + \pi$ , the crank radius  $\lambda_{r4}$  is set equal to the dimensionless limiting radius  $\lambda_{rc}$ , i.e.

$$\lambda_{r4} \Big|_{\varphi_1 = \varphi_c} = \lambda_{rc} \quad (15)$$

and the rate of change of  $\lambda_{r4}$  is set equal to zero, i.e.

$$\lambda'_{r4} \Big|_{\varphi_1 = \varphi_c} = 0 \quad (16)$$

Thereby, the total number of the conditions given by Eqs.(13)–(16) equals  $n = 10$ . These conditions lead to the following system of equations with respect to the coefficients  $a_i$  in Eq.(12):

$$\begin{pmatrix} 1 & \varphi_{1\Sigma} & \varphi_{1\Sigma}^2 & \varphi_{1\Sigma}^3 & \varphi_{1\Sigma}^4 & \varphi_{1\Sigma}^5 & \varphi_{1\Sigma}^6 & \varphi_{1\Sigma}^7 & \varphi_{1\Sigma}^8 & \varphi_{1\Sigma}^9 \\ 0 & 1 & 2\varphi_{1\Sigma} & 3\varphi_{1\Sigma}^2 & 4\varphi_{1\Sigma}^3 & 5\varphi_{1\Sigma}^4 & 6\varphi_{1\Sigma}^5 & 7\varphi_{1\Sigma}^6 & 8\varphi_{1\Sigma}^7 & 9\varphi_{1\Sigma}^8 \\ 0 & 0 & 2 & 6\varphi_{1\Sigma} & 12\varphi_{1\Sigma}^2 & 20\varphi_{1\Sigma}^3 & 30\varphi_{1\Sigma}^4 & 42\varphi_{1\Sigma}^5 & 56\varphi_{1\Sigma}^6 & 72\varphi_{1\Sigma}^7 \\ 0 & 0 & 0 & 6 & 24\varphi_{1\Sigma} & 60\varphi_{1\Sigma}^2 & 120\varphi_{1\Sigma}^3 & 210\varphi_{1\Sigma}^4 & 336\varphi_{1\Sigma}^5 & 504\varphi_{1\Sigma}^6 \\ 1 & \varphi_e & \varphi_e^2 & \varphi_e^3 & \varphi_e^4 & \varphi_e^5 & \varphi_e^6 & \varphi_e^7 & \varphi_e^8 & \varphi_e^9 \\ 0 & 1 & 2\varphi_e & 3\varphi_e^2 & 4\varphi_e^3 & 5\varphi_e^4 & 6\varphi_e^5 & 7\varphi_e^6 & 8\varphi_e^7 & 9\varphi_e^8 \\ 0 & 0 & 2 & 6\varphi_e & 12\varphi_e^2 & 20\varphi_e^3 & 30\varphi_e^4 & 42\varphi_e^5 & 56\varphi_e^6 & 72\varphi_e^7 \\ 0 & 0 & 0 & 6 & 24\varphi_e & 60\varphi_e^2 & 120\varphi_e^3 & 210\varphi_e^4 & 336\varphi_e^5 & 504\varphi_e^6 \\ 1 & \varphi_c & \varphi_c^2 & \varphi_c^3 & \varphi_c^4 & \varphi_c^5 & \varphi_c^6 & \varphi_c^7 & \varphi_c^8 & \varphi_c^9 \\ 0 & 1 & 2\varphi_c & 3\varphi_c^2 & 4\varphi_c^3 & 5\varphi_c^4 & 6\varphi_c^5 & 7\varphi_c^6 & 8\varphi_c^7 & 9\varphi_c^8 \end{pmatrix} \begin{pmatrix} a_1 \\ a_2 \\ a_3 \\ a_4 \\ a_5 \\ a_6 \\ a_7 \\ a_8 \\ a_9 \\ a_{10} \end{pmatrix} = \begin{pmatrix} \lambda_{r3} |_{\varphi_{1\Sigma}} \\ \lambda'_{r3} |_{\varphi_{1\Sigma}} \\ \lambda''_{r3} |_{\varphi_{1\Sigma}} \\ \lambda_{r1} |_0 \\ \lambda'_{r1} |_0 \\ \lambda''_{r1} |_0 \\ \lambda_{r1} |_0 \\ \lambda'_{r1} |_0 \\ \lambda_{rc} \\ 0 \end{pmatrix} \quad (17)$$

where  $\varphi_e$  stands for  $2\pi$  for shorter notation.

Now it is turn to determine the maximum pressure angle  $\nu_{\max}$  and minimum curvature radius  $\rho_{\min}$  of the cam profile for each zone and compare them to the allowable values  $[\nu]$  and  $[\rho]$ , respectively.

#### 4.1. Limitation condition for the maximum pressure angle

*Zone I.* Substitution of Eq.(11) into Eq.(6) results in the pressure angle  $\nu = \varphi_1$ . Since the crank rotation angle  $\varphi_1$  changes from 0 to  $\Delta\varphi$ , it is true that the maximum pressure angle equals  $\nu_{\max} = \Delta\varphi$ . The condition of Eq.(7) is thus fulfilled if  $\Delta\varphi \leq [\nu]$  or, taking account of Eq.(1) and Eq.(2), if

$$k_{at} \leq \frac{2z}{\pi(z-2)} [\nu] \quad (18)$$

Fig.5a shows the range of the additional dwell coefficient  $k_{at}$  that satisfies Eq.(18). The coefficient  $k_{at}$  can take any value between 0 and 0.7 for  $z \in \{3,4\}$ . As the number  $z$  of slots increases, the upper limit of the range decreases. For  $z = 15$ , it equals 0.417 at  $[\nu] = 32.5^\circ$  and 0.532 at  $[\nu] = 41.6^\circ$

[insert Figure 5.]

*Zone II.* Substitution of Eq.(3) and Eq.(4) into Eq.(6) allows deriving the expression of the pressure angle  $\nu$  in the form

$$\tan \nu = \frac{\sin(\varphi_1 + \varphi_2) \sin(\pi/z - \varphi_2) - \varphi_2' \cos(\pi/z + \varphi_1)}{\cos(\varphi_1 + \varphi_2) \sin(\pi/z - \varphi_2)} \quad (19)$$

Assume that the wheel moves according to the cycloidal law

$$a_k = k - \frac{\sin(2\pi k)}{2\pi} \quad (20)$$

which is widespread in the cyclic mechanisms, providing zero angular acceleration of the wheel in its extreme positions, i.e. at the start and end of its motion period.

The maximum pressure angle  $\nu_{\max}$  is determined based on Eq.(19) and Eq.(20). Fig.5b shows the corresponding range of the coefficient  $k_{at}$  satisfying Eq.(7). As in the case of zone I, the coefficient  $k_{at}$  can be arbitrary from 0 to 0.7 for  $z \in \{3,4\}$ . As the number  $z$  increases, the upper

limit of the range decreases. For  $z = 15$ , it equals 0.375 at  $[\nu] = 32.5^\circ$  and 0.506 at  $[\nu] = 41.6^\circ$ . Comparison of Fig.5a and Fig.5b shows that the coefficient  $k_{at}$  is smaller in the zone II for any  $z$ .

*Zone III.* Since the zones I and III are symmetrical about the vertical axis (see Fig.4), similar conclusions can be drawn here as for the zone I.

*Zone IV.* The crank radius  $\lambda_{r4}$  represents the polynomial of Eq.(12) with the coefficients  $a_i$  satisfying Eq.(17). The dependence of the maximum pressure angle  $\nu_{max}$  on the number  $z$  and limiting radius  $\lambda_{rc}$  is obtained based on Eq.(6). Fig.6 shows the relevant data for the limiting radius  $\lambda_{rc}$  that changes from 1 to 2.2 with step 0.2. It is seen that for  $[\nu] = 32.5^\circ$ , the condition of Eq.(7) is fulfilled at  $1 \leq \lambda_{rc} \leq 2$  and any  $z$ , as well as at  $\lambda_{rc} = 2.2$  and  $z \leq 7$ . For  $[\nu] = 41.6^\circ$ , the entire range of  $\lambda_{rc}$  satisfies the condition of Eq.(7). Note that the maximum pressure angle  $\nu_{max}$  increases with increasing  $\lambda_{rc}$ .

[insert Figure 6.]

Summarising the results for all zones leads to the conclusion that the condition of Eq.(7) limiting the maximum pressure angle  $\nu_{max}$  can be fulfilled for any  $z$ . As the number  $z$  increases, the upper limit of the coefficient  $k_{at}$  decreases. For  $[\nu] = 32.5^\circ$ , it equals 0.7 at  $z = 3$  and 0.375 at  $z = 15$ , whilst for  $[\nu] = 41.6^\circ$ , it is about 1.3 times larger. The coefficient  $k_{at}$  should be chosen according to the results obtained for the zone II (see Fig.5b). Additionally, the limiting radius  $\lambda_{rc}$  should be specified as small as possible to reduce the maximum pressure angle  $\nu_{max}$ .

#### 4.2. Limitation condition of the minimum curvature radius of the cam profile

*Zone I.* Since the path  $AA_1$  of the driving pin is linear (see Fig.4), the curvature radius of the cam profile is infinitely large.

*Zone II.* Substitution of Eq.(20) into Eqs.(3)–(5) allows determining the allowable curvature radius  $[\rho]$  of the cam profile due to Eq.(8) and the minimum curvature radius  $\rho_{min}$  of the cam profile due to Eq.(9). Fig.7 shows the range of the coefficient  $k_{at}$  satisfying the condition of Eq.(10) in dependence on the number  $z$ . The analysis reveals that for  $[\nu] = 32.5^\circ$ , the synthesis of the driving pin path is possible at  $z \geq 4$ . The coefficient  $k_{at}$  is in range from 0 to 0.29 at  $4 \leq z \leq 13$  and in range from 0 to 0.28 at  $z \in \{14,15\}$ . As for  $[\nu] = 41.6^\circ$ , the condition of Eq.(10) is fulfilled for any  $z$ . The upper limit of the coefficient  $k_{at}$  equals 0.34 at  $z = 3$ , 0.37 at  $z \in \{4,5,6,13,14,15\}$  and 0.38 at  $7 \leq z \leq 12$ .

[insert Figure 7.]

*Zone III.* Similar conclusions are valid as for the zone I due to the symmetry of the zones I and III about the vertical axis (see Fig.4).

*Zone IV.* The crank radius  $\lambda_{r4}$  is described by the polynomial Eq.(12) with the coefficients  $a_i$  satisfying Eq.(17). Fig.8 shows the allowable curvature radius  $[\rho]$  of the cam profile determined based on Eq.(8). Fig.9 shows the minimum curvature radius  $\rho_{min}$  of the cam profile determined by Eq.(9).

[insert Figure 8.]

[insert Figure 9.]

Fig.8 and Fig.9 suggest that the condition of Eq.(10) is fulfilled almost in the entire ranges of the number  $z$  and limiting radius  $\lambda_{rc}$ . For  $[\nu] = 32.5^\circ$  and  $\lambda_{rc} = 2.2$ , this condition is fulfilled at  $z$





1  
2  
3  $\leq 10$ . The limiting radius  $\lambda_{rc}$  should take the smallest possible value to reduce the geometric  
4 dimensions of the mechanism whilst providing a single-sign curvature path of the driving pin.

5 Thereby, Figs.5–9 outline the set of the groove cam Geneva mechanisms that provide the  
6 double locking of the wheel at its dwell-to-motion and motion-to-dwell transitions, absence of soft  
7 impacts in the extreme positions and significantly wider range of the operating time coefficient  $k_w$   
8 compared to the conventional Geneva mechanisms. It should be noted that the developed method is  
9 not limited by the type of function given by Eq.(20) and can be applied for arbitrary law of motion  
10 of the wheel.  
11

## 12 5. Synthesis algorithm

13 The theoretical results obtained in Sections 2–4 can be combined into one algorithm  
14 presented in Fig.10. At the first stage, the number  $z$  of slots and the operating time coefficient  $k_w$   
15 are determined by Eq.(2). At the second stage, the cam profile is checked for the maximum pressure  
16 angle  $\nu_{max}$  due to Eq.(7). As mentioned in Section 4.1, the symmetry of the cam profile in the zones  
17 I and III should be taken into consideration. At the third stage, the cam profile is checked for the  
18 minimum curvature radius  $\rho_{min}$  due to Eq.(10). Remind that the check is not performed for the  
19 zones I and III where the driving pin path is linear. If at least one of the conditions Eq.(7) and  
20 Eq.(10) is not fulfilled, the algorithm returns to the first stage.  
21

22 Repetition of the first three stages leads to the fourth stage which consists in forming the set  
23 of pairs  $z$  and  $k_w$  that satisfy the main and additional conditions of synthesis. The fifth stage is  
24 selection of the optimum solution. In general, a smaller value of  $k_w$  corresponds to a higher  
25 productivity of the machine employing the groove cam Geneva mechanism but also to higher  
26 inertial loads on the mechanism. Therefore, a dynamic analysis of the mechanism considering  
27 inertial masses attached to the wheel is necessary to evaluate the margin of strength that can be  
28 sacrificed in favour of productivity. At the sixth stage, the cam profile is drawn based on the  
29 synthesised path of the driving pin.  
30

31 Since in the present study the centre  $C$  of the roller follower 5 is assumed to coincide with  
32 the centre  $A$  of the driving pin 4 (see Fig.2), i.e. the cam profile is identical to the path of the centre  
33  $A$ , the final stage of the algorithm does not require calculations. In the general case, this assumption  
34 is not true, and the cam profile is to be drawn based on the path of the driving pin centre  $A$ .  
35 Obviously, the expressions derived in Sections 3 and 4 become more cumbersome in this case.  
36 Nonetheless, the general approach presented in Section 2 and summarised by the algorithm in  
37 Fig.10 remains valid.  
38

39  
40  
41  
42 [insert Figure 10.]  
43  
44

## 45 6. Method application

46 For example, consider a problem of synthesising the Geneva mechanism with operating time  
47 coefficient  $k_w = 0.3$ . Fig.3 shows that none of the number  $z$  of slots satisfies  $k_w = 0.3$  and  $k_{at} = 0$ ,  
48 i.e. the conventional Geneva mechanism cannot provide the required value of  $k_w$ . Find the solution  
49 using the algorithm proposed in Fig.10, accepting the allowable pressure angle equal to  $[\nu] = 41.6^\circ$ .

50 Table 1 presents the pairs  $z$  and  $k_{at}$  that provide  $k_w = 0.3$  due to Eq.(2). The set of solutions  
51 is thus  $4 \leq z \leq 15$ . Fig.5 and Fig.6 show that the condition of Eq.(7) is fulfilled in the zones I–IV  
52 for any values of  $z$  in the entire range of the limiting radius  $\lambda_{rc}$ , i.e. this condition does not narrow  
53 down the set of solutions. On the other hand, due to Fig.7, the condition of Eq.(10) is fulfilled in the  
54 zone II at  $z \leq 7$ . Comparison of Fig.8 and Fig.9 suggests no additional limitations in the zone IV.  
55 Thereby, the set of solutions is narrowed down by Eq.(10) to  $4 \leq z \leq 7$ . Fig.11a presents the  
56 synthesised paths of the driving pin for the limit values of  $z$  at  $\lambda_{rc} = 1$ . The solution  $z = 4$  provides  
57 minimum inertia load on the mechanism, whereas the solution  $z = 7$  maximises the machine  
58 productivity.  
59  
60

Table 1. Pairs of the number  $z$  of slots and additional dwell coefficient  $k_{at}$  providing  $k_w = 0.3$ 

$z$	4	5	6	7	8	9	10	11	12	13	14	15
$k_{at}$	0.0769	0.231	0.308	0.354	0.385	0.407	0.423	0.436	0.446	0.456	0.462	0.468

Now consider another problem that consists in synthesising the Geneva mechanism with specified number of slots  $z = 8$ . For the sake of variety, the allowable pressure angle is set equal to  $[\nu] = 32.5^\circ$  in this example.

Fig.3 outlines the infinite set of solutions for  $z = 8$  in the form of  $k_{at}$  ranging between 0 to 0.7. The check of Eq.(7) shows that  $k_{at}$  is limited from above by 0.48 in the zones I and III, as shown in Fig.5a, and by 0.46 in the zone II, as shown in Fig.5b. Due to Fig.6 for the zone IV, the limiting radius  $\lambda_{rc}$  may vary between 1 and 2. Further, the check of Eq.(10) shows that  $k_{at}$  is limited from above by 0.29 in the zone II, as shown in Fig.7, whilst there are no additional limitations in the zone IV, as shown in Fig.8 and Fig.9. The set of solutions is thereby limited by Eq.(7) and Eq.(10) to the range  $0 \leq k_{at} \leq 0.29$ . Fig.11b shows the synthesised paths of the driving pin for the limit values of  $k_{at}$  at  $\lambda_{rc} = 1$ . The solution  $k_{at} = 0$  has the same operating time coefficient  $k_w = 0.6$  as the conventional Geneva mechanism. In contrast, the solution  $k_{at} = 0.29$  corresponds to  $k_w = 0.37$ , i.e. the groove cam Geneva mechanism synthesised by the algorithm in Fig.10 allows improving the machine productivity by  $(1 + 0.6)/(1 + 0.37) \approx 1.17$  times.

[insert Figure 11.]

## 7. Conclusions

A synthesis method for the groove cam external Geneva mechanisms with increased dwell period is developed which provides the required law of motion of the wheel with account of the conditions limiting the maximum pressure angle  $\nu_{max}$  and minimum curvature radius  $\rho_{min}$  of the cam profile.

It is shown that unlike the conventional Geneva mechanisms, the synthesised groove cam Geneva mechanisms enable:

- arbitrary law of motion of the wheel;
- double locking of the wheel at its dwell-to-motion and motion-to-dwell transitions;
- absence of soft impacts in the extreme positions;
- significantly wider range of the operating time coefficient  $k_w$ .

The dimensionless analysis performed for the cycloidal law of motion, number  $z$  of slots in range from 3 to 15, additional dwell coefficient  $k_{at}$  in range from 0 to 0.7 shows that the operating time coefficient  $k_w$  is provided in range from 0.053 to 0.765. The advantages of the synthesised groove cam Geneva mechanisms over the conventional Geneva mechanisms are clearly illustrated by the numerical examples.

## Declaration of conflicting interests

The authors declare that there is no conflict of interest.

## Funding

The authors received no financial support for the research, authorship, and/or publication of this article.

## References

1. Bickford JH. *Mechanisms for intermittent motion*. New York: Industrial Press Inc., 1972, pp.127–138.

2. Chironis NP, Nicholas P. *Mechanisms and mechanical devices sourcebook*. New York: McGraw-Hill, 1991.
3. Prajapati A, Patel C, Pankhania D, et al. Review on Geneva mechanism and its application. *Int J Adv Eng Res Dev* 2017; 4 (2): 425–429.
4. Beltz RK, Hurst JC. Peristaltic pump metering and dispensing system. *Technical Digest - Western Electric Company*, 1975, no.37, pp.3–4.
5. Pazouki ME, Jones JR. The kinematic synthesis of a linkage driven Geneva mechanism. *Mech Mach Theory* 1982; 17 (3): 221–228.
6. Meyer G. A tested method for precise intermittent motion. *Mach Des* 1988; 60 (1): 140–143.
7. Egorov OD, Nadezhdin IV. Use of Geneva mechanisms in industrial robots. *Sov Eng Res* 1988; 8 (11): 134–137.
8. Lee JJ, Cho CC. Improving kinematic and structural performance of Geneva mechanism using the optimal control method. *Proc Inst Mech Eng C J Mech Eng Sci* 2002; 216 (7): 761–774.
9. Kali Sindhur P, Karthik Y, vijay T, et al. Cutting mechanism by giving through Geneva mechanism. *Int J Innov Sci Eng Technol* 2015; 2 (4): 1172–1175.
10. Ujam AJ, Ejeogo G, Onyeneho KC. Development and application of Geneva mechanism for bottle washing. *Am J Eng Res* 2015; 4 (11): 63–73.
11. Zhang E, Wang L. Parametric design and motion analysis of Geneva wheel mechanism based on the UG NX8.5. In: *International Conference on Manufacturing Engineering and Intelligent Materials*, Advances in Engineering, 2017, vol.100, pp.352–356.
12. Sepahpour B. *Kinematic and kinetic analysis of Geneva mechanisms and their applications to synchronization of motion*. PhD Thesis, New Jersey Institute of Technology, 1994.
13. Figliolini G, Rea P, Angeles J. The pure-rolling cam-equivalent of the Geneva mechanism. *Mech Mach Theory* 2006; 41 (11): 1320–1335.
14. Shaohua S, Jifei C. Kinematic analysis on series combined mechanism of elliptic gear and outer Geneva. *Appl Mech Mater* 2013; 312: 42–46.
15. Dijkstra EA. Jerk-free Geneva wheel driving. *J Mech* 1966; 1 (3–4): 235–280.
16. Bagci C. Synthesis of double-crank driven mechanisms with adjustable motion and dwell time ratios. *Mech Mach Theory* 1977; 12 (6): 619–638.
17. Yang AT, Hsia LM. Multistage geared Geneva mechanism. *Trans ASME J Mech Des* 1979; 101 (1): 41–46.
18. Fenton RG. Geneva mechanisms connected in series. *Trans ASME J Manuf Sci Eng* 1975; 97: 603–608.
19. Al-Sabeeh AK. Double crank external Geneva mechanism. *Trans ASME J Mech Des* 1993; 115: 666–670.
20. Figliolini G, Rea P. Effects of the design parameters on the synthesis of Geneva mechanisms. *Proc Inst Mech Eng C J Mech Eng Sci* 2012; 227 (9): 2000–2009.
21. Yang AT, Hsia LM. Multistage geared Geneva mechanism. *Trans ASME J Mech Des* 1979; 101: 41–46.
22. Sujana VA, Meggiolaro MA. Dynamic optimization of Geneva mechanisms. In: *International Conference on Gearing, Transmissions and Mechanical Systems*, 2000, pp.687–696.
23. Sadek KSH., Lloyd JL, Smith MR. A new design of Geneva drive to reduce shock loading. *Mech Mach Theory* 1990; 25: 589–595.
24. Cheng CY, Lin Y. Improving dynamic performance of the Geneva mechanism using non-linear spring elements. *Mech Mach Theory* 1995; 30: 119–129.
25. Fenton RG, Zhang Y, Xu J. Development of a new Geneva mechanism with improved kinematic characteristics. *Trans ASME J Mech Des* 1991; 113 (1): 40–45.
26. Lee HP. Design of a Geneva mechanism with curved slots using parametric polynomials. *Mech Mach Theory* 1998; 33 (3): 321–329.
27. Lee JJ, Huang KF. Geometry analysis and optimal design of Geneva mechanisms with curved slots. *Proc Inst Mech Eng C J Mech Eng Sci* 2004; 218 (4): 449–458.

- 1  
2  
3 28. Lee JJ, Jan BH. Design of Geneva mechanisms with curved slots for non-undercutting  
4 manufacturing. *Mech Mach Theory* 2009; 44 (6): 1192–1200.  
5 29. Li HT. Design of a new kind of curved groove on Geneva mechanism. *J China Agric Univ*  
6 2005; 10: 62–65.  
7 30. DuMont CL, Kurtz AF, Silverstein BD, et al. Design improvement for motion picture film  
8 projectors. In: *143rd Technical Conference and Exhibition*, New York, 2001, pp.785–791.  
9 31. Zhang J, Sun S, Tuan HA. Optimization design and analysis of rotary indexing mechanism of  
10 tool magazine in machining center. *Jordan J Mech Ind Eng* 2020; 14 (1): 1–6.  
11 32. Heidari M, Atai AA, Shariat Panahi M. An improved Geneva mechanism for optimal kinematic  
12 performance. *Proc Inst Mech Eng C J Mech Eng Sci* 2012; 226 (6): 1515–1525.  
13 33. Polyudov OM. *Mechanics of printing machines*. Kyiv: NMKVO, 1991.  
14 34. Uicker JJ, Pennock GR, Shigley JE. *Theory of machines and mechanisms*. 5th ed. New York:  
15 Oxford University Press, 2017.  
16  
17  
18  
19  
20  
21  
22  
23  
24  
25  
26  
27  
28  
29  
30  
31  
32  
33  
34  
35  
36  
37  
38  
39  
40  
41  
42  
43  
44  
45  
46  
47  
48  
49  
50  
51  
52  
53  
54  
55  
56  
57  
58  
59  
60

For Peer Review

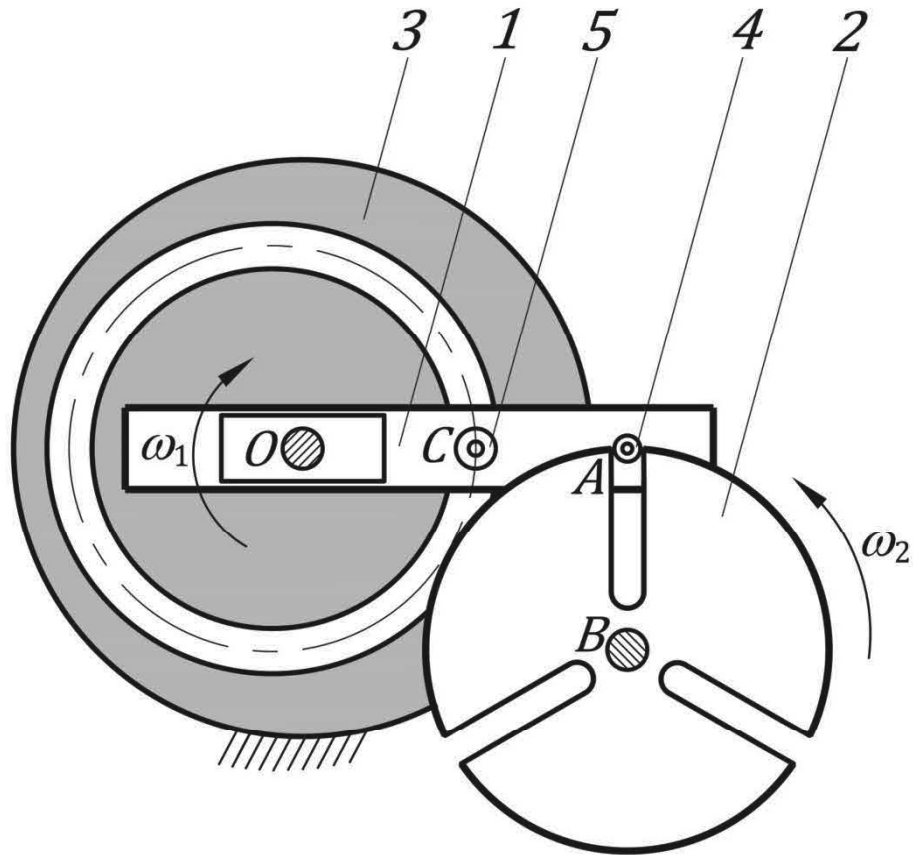


Figure 1. General schematic of the groove cam Geneva mechanism: input crank 1, output wheel 2, groove cam 3, driving pin 4 and roller follower 5

80x80mm (600 x 600 DPI)

Downloaded from mostwiedzy.pl  
MOST WIEDZY

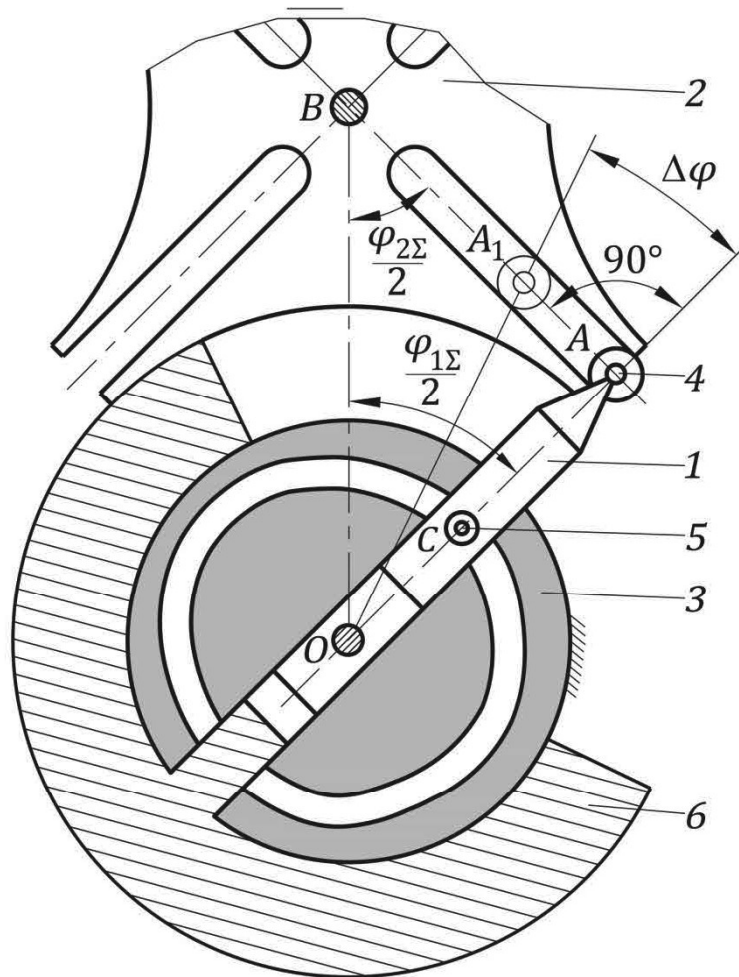


Figure 2. Detailed schematic of the groove cam Geneva mechanism: input crank 1, output wheel 2, groove cam 3, driving pin 4 and roller follower 5, locking ring 6

119x119mm (600 x 600 DPI)

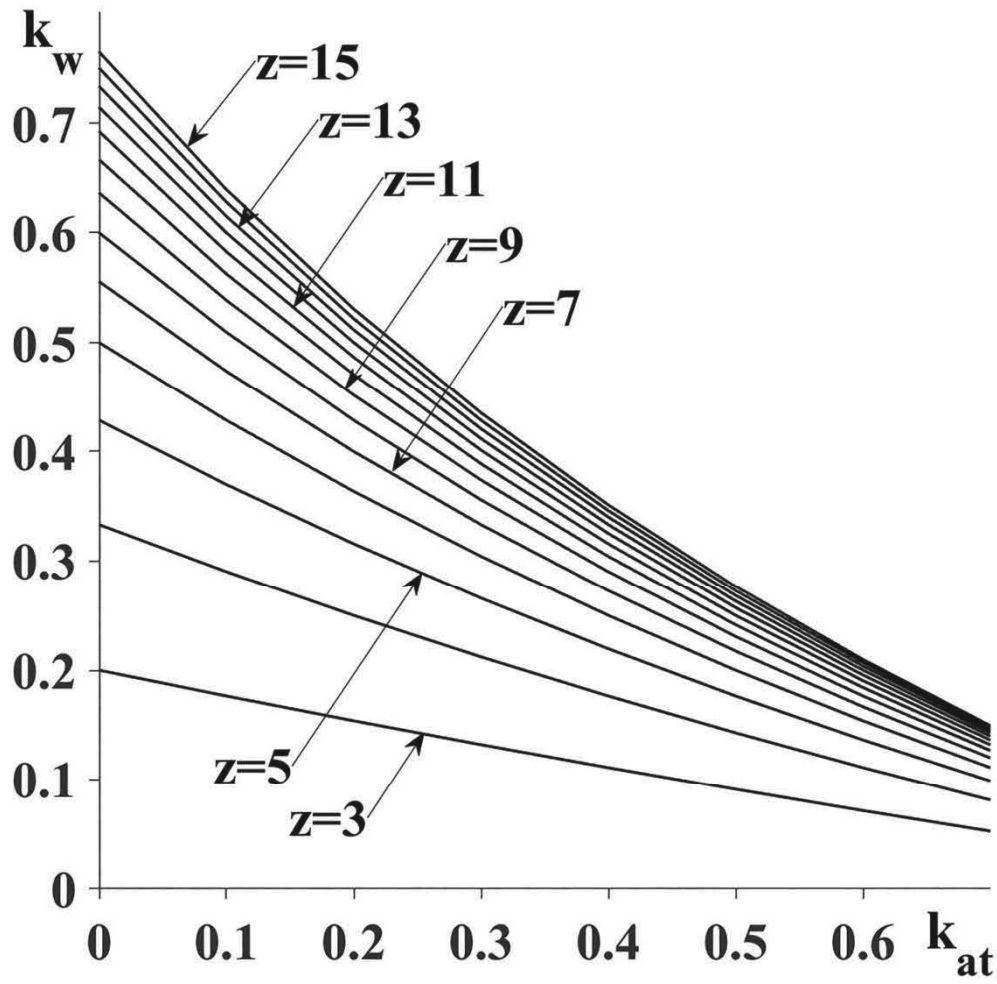


Figure 3. Dependence of the operating time coefficient  $k_w$  on the additional dwell coefficient  $k_{at}$  and number  $z$  of slots

80x80mm (600 x 600 DPI)

Downloaded from mostwiedzy.pl

MOST WIEDZY

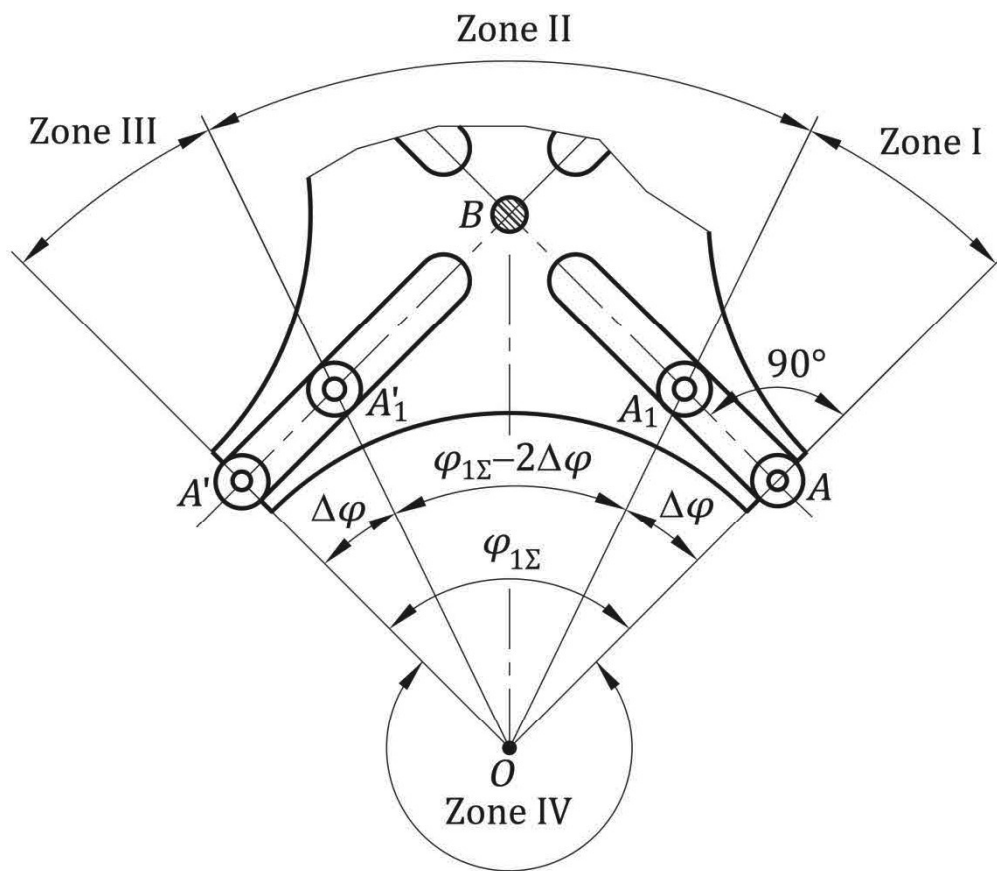


Figure 4. Characteristic zones of the crank rotation

119x119mm (600 x 600 DPI)

1  
2  
3  
4  
5  
6  
7  
8  
9  
10  
11  
12  
13  
14  
15  
16  
17  
18  
19  
20  
21  
22  
23  
24  
25  
26  
27  
28  
29  
30  
31  
32  
33  
34  
35  
36  
37  
38  
39  
40  
41  
42  
43  
44  
45  
46  
47  
48  
49  
50  
51  
52  
53  
54  
55  
56  
57  
58  
59  
60  
61  
62  
63  
64  
65  
66  
67  
68  
69  
70  
71  
72  
73  
74  
75  
76  
77  
78  
79  
80  
81  
82  
83  
84  
85  
86  
87  
88  
89  
90  
91  
92  
93  
94  
95  
96  
97  
98  
99  
100  
101  
102  
103  
104  
105  
106  
107  
108  
109  
110  
111  
112  
113  
114  
115  
116  
117  
118  
119  
120  
121  
122  
123  
124  
125  
126  
127  
128  
129  
130  
131  
132  
133  
134  
135  
136  
137  
138  
139  
140  
141  
142  
143  
144  
145  
146  
147  
148  
149  
150  
151  
152  
153  
154  
155  
156  
157  
158  
159  
160  
161  
162  
163  
164  
165  
166  
167  
168  
169  
170  
171  
172  
173  
174  
175  
176  
177  
178  
179  
180  
181  
182  
183  
184  
185  
186  
187  
188  
189  
190  
191  
192  
193  
194  
195  
196  
197  
198  
199  
200  
201  
202  
203  
204  
205  
206  
207  
208  
209  
210  
211  
212  
213  
214  
215  
216  
217  
218  
219  
220  
221  
222  
223  
224  
225  
226  
227  
228  
229  
230  
231  
232  
233  
234  
235  
236  
237  
238  
239  
240  
241  
242  
243  
244  
245  
246  
247  
248  
249  
250  
251  
252  
253  
254  
255  
256  
257  
258  
259  
260  
261  
262  
263  
264  
265  
266  
267  
268  
269  
270  
271  
272  
273  
274  
275  
276  
277  
278  
279  
280  
281  
282  
283  
284  
285  
286  
287  
288  
289  
290  
291  
292  
293  
294  
295  
296  
297  
298  
299  
300  
301  
302  
303  
304  
305  
306  
307  
308  
309  
310  
311  
312  
313  
314  
315  
316  
317  
318  
319  
320  
321  
322  
323  
324  
325  
326  
327  
328  
329  
330  
331  
332  
333  
334  
335  
336  
337  
338  
339  
340  
341  
342  
343  
344  
345  
346  
347  
348  
349  
350  
351  
352  
353  
354  
355  
356  
357  
358  
359  
360  
361  
362  
363  
364  
365  
366  
367  
368  
369  
370  
371  
372  
373  
374  
375  
376  
377  
378  
379  
380  
381  
382  
383  
384  
385  
386  
387  
388  
389  
390  
391  
392  
393  
394  
395  
396  
397  
398  
399  
400  
401  
402  
403  
404  
405  
406  
407  
408  
409  
410  
411  
412  
413  
414  
415  
416  
417  
418  
419  
420  
421  
422  
423  
424  
425  
426  
427  
428  
429  
430  
431  
432  
433  
434  
435  
436  
437  
438  
439  
440  
441  
442  
443  
444  
445  
446  
447  
448  
449  
450  
451  
452  
453  
454  
455  
456  
457  
458  
459  
460  
461  
462  
463  
464  
465  
466  
467  
468  
469  
470  
471  
472  
473  
474  
475  
476  
477  
478  
479  
480  
481  
482  
483  
484  
485  
486  
487  
488  
489  
490  
491  
492  
493  
494  
495  
496  
497  
498  
499  
500



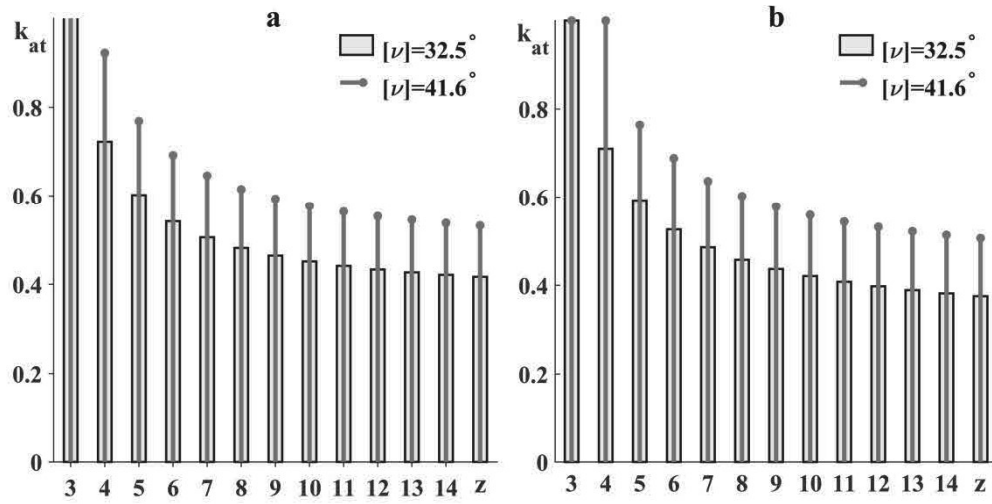


Figure 5. Range of the additional dwell coefficient  $k_{at}$  depending on the number  $z$  of slots: (a) zone I; (b) zone II

159x80mm (600 x 600 DPI)

Downloaded from mostwiedzy.pl

MOST WIEDZY

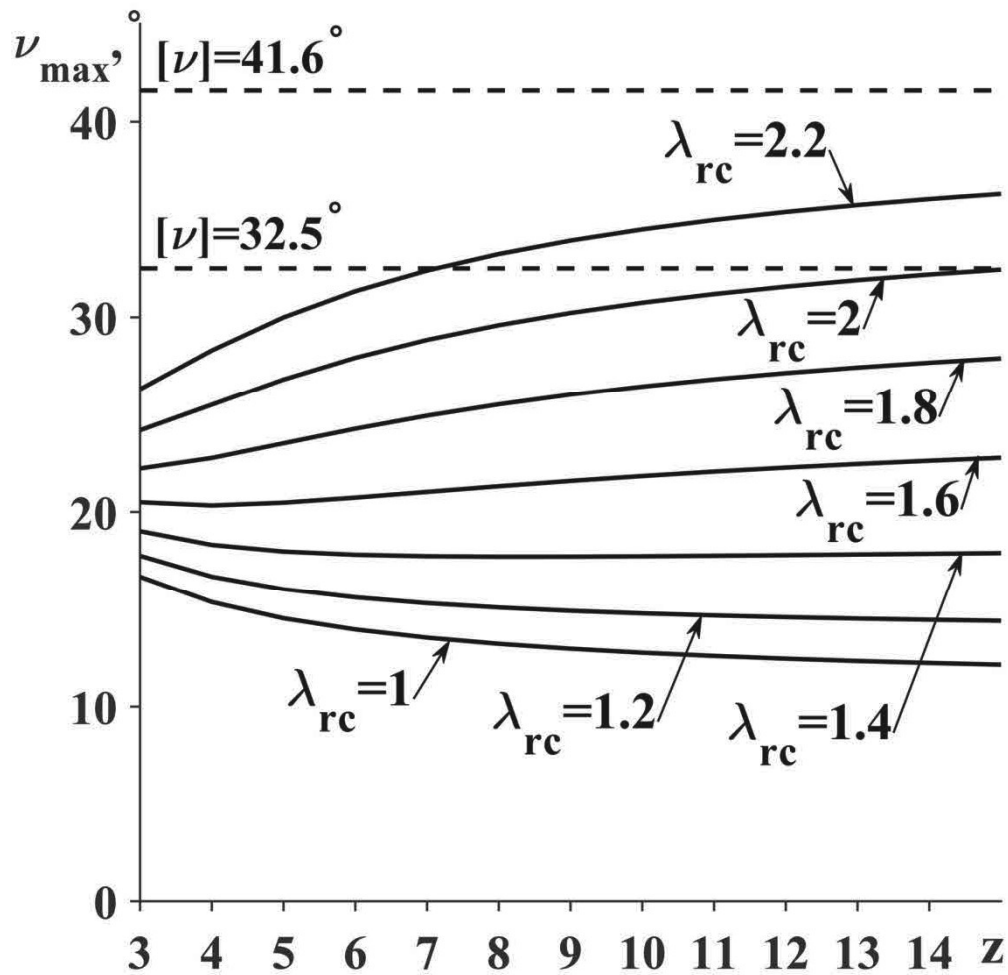


Figure 6. Dependence of the maximum pressure angle  $\nu_{\max}$  on the number  $z$  of slots and limiting radius  $\lambda_{rc}$  in the zone IV

80x80mm (600 x 600 DPI)

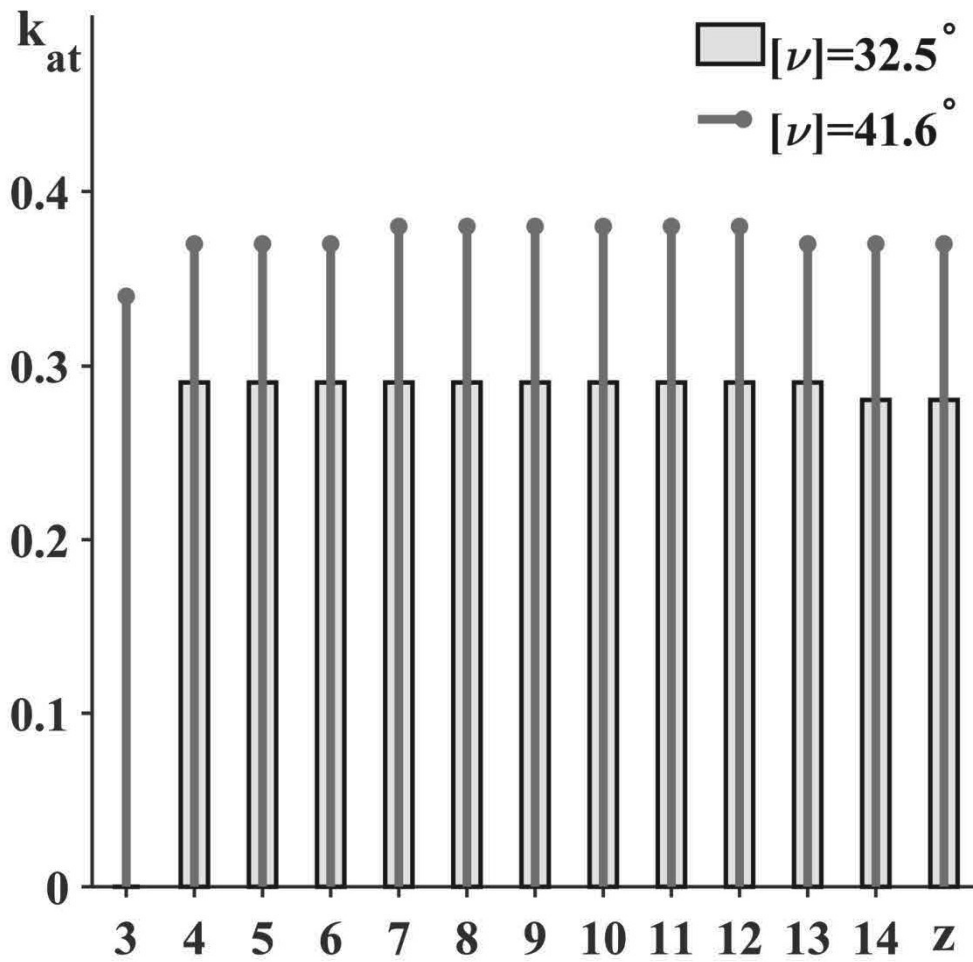


Figure 7. Range of the additional dwell coefficient  $k_{at}$  depending on the number  $z$  of slots in the zone II

80x80mm (600 x 600 DPI)

36  
37  
38  
39  
40  
41  
42  
43  
44  
45  
46  
47  
48  
49  
50  
51  
52  
53  
54  
55  
56  
57  
58  
59  
60  
61  
62  
63  
64  
65  
66  
67  
68  
69  
70  
71  
72  
73  
74  
75  
76  
77  
78  
79  
80  
81  
82  
83  
84  
85  
86  
87  
88  
89  
90  
91  
92  
93  
94  
95  
96  
97  
98  
99  
100  
101  
102  
103  
104  
105  
106  
107  
108  
109  
110  
111  
112  
113  
114  
115  
116  
117  
118  
119  
120  
121  
122  
123  
124  
125  
126  
127  
128  
129  
130  
131  
132  
133  
134  
135  
136  
137  
138  
139  
140  
141  
142  
143  
144  
145  
146  
147  
148  
149  
150  
151  
152  
153  
154  
155  
156  
157  
158  
159  
160  
161  
162  
163  
164  
165  
166  
167  
168  
169  
170  
171  
172  
173  
174  
175  
176  
177  
178  
179  
180  
181  
182  
183  
184  
185  
186  
187  
188  
189  
190  
191  
192  
193  
194  
195  
196  
197  
198  
199  
200  
201  
202  
203  
204  
205  
206  
207  
208  
209  
210  
211  
212  
213  
214  
215  
216  
217  
218  
219  
220  
221  
222  
223  
224  
225  
226  
227  
228  
229  
230  
231  
232  
233  
234  
235  
236  
237  
238  
239  
240  
241  
242  
243  
244  
245  
246  
247  
248  
249  
250  
251  
252  
253  
254  
255  
256  
257  
258  
259  
260  
261  
262  
263  
264  
265  
266  
267  
268  
269  
270  
271  
272  
273  
274  
275  
276  
277  
278  
279  
280  
281  
282  
283  
284  
285  
286  
287  
288  
289  
290  
291  
292  
293  
294  
295  
296  
297  
298  
299  
300  
301  
302  
303  
304  
305  
306  
307  
308  
309  
310  
311  
312  
313  
314  
315  
316  
317  
318  
319  
320  
321  
322  
323  
324  
325  
326  
327  
328  
329  
330  
331  
332  
333  
334  
335  
336  
337  
338  
339  
340  
341  
342  
343  
344  
345  
346  
347  
348  
349  
350  
351  
352  
353  
354  
355  
356  
357  
358  
359  
360  
361  
362  
363  
364  
365  
366  
367  
368  
369  
370  
371  
372  
373  
374  
375  
376  
377  
378  
379  
380  
381  
382  
383  
384  
385  
386  
387  
388  
389  
390  
391  
392  
393  
394  
395  
396  
397  
398  
399  
400  
401  
402  
403  
404  
405  
406  
407  
408  
409  
410  
411  
412  
413  
414  
415  
416  
417  
418  
419  
420  
421  
422  
423  
424  
425  
426  
427  
428  
429  
430  
431  
432  
433  
434  
435  
436  
437  
438  
439  
440  
441  
442  
443  
444  
445  
446  
447  
448  
449  
450  
451  
452  
453  
454  
455  
456  
457  
458  
459  
460  
461  
462  
463  
464  
465  
466  
467  
468  
469  
470  
471  
472  
473  
474  
475  
476  
477  
478  
479  
480  
481  
482  
483  
484  
485  
486  
487  
488  
489  
490  
491  
492  
493  
494  
495  
496  
497  
498  
499  
500  
501  
502  
503  
504  
505  
506  
507  
508  
509  
510  
511  
512  
513  
514  
515  
516  
517  
518  
519  
520  
521  
522  
523  
524  
525  
526  
527  
528  
529  
530  
531  
532  
533  
534  
535  
536  
537  
538  
539  
540  
541  
542  
543  
544  
545  
546  
547  
548  
549  
550  
551  
552  
553  
554  
555  
556  
557  
558  
559  
560  
561  
562  
563  
564  
565  
566  
567  
568  
569  
570  
571  
572  
573  
574  
575  
576  
577  
578  
579  
580  
581  
582  
583  
584  
585  
586  
587  
588  
589  
590  
591  
592  
593  
594  
595  
596  
597  
598  
599  
600  
601  
602  
603  
604  
605  
606  
607  
608  
609  
610  
611  
612  
613  
614  
615  
616  
617  
618  
619  
620  
621  
622  
623  
624  
625  
626  
627  
628  
629  
630  
631  
632  
633  
634  
635  
636  
637  
638  
639  
640  
641  
642  
643  
644  
645  
646  
647  
648  
649  
650  
651  
652  
653  
654  
655  
656  
657  
658  
659  
660  
661  
662  
663  
664  
665  
666  
667  
668  
669  
670  
671  
672  
673  
674  
675  
676  
677  
678  
679  
680  
681  
682  
683  
684  
685  
686  
687  
688  
689  
690  
691  
692  
693  
694  
695  
696  
697  
698  
699  
700  
701  
702  
703  
704  
705  
706  
707  
708  
709  
710  
711  
712  
713  
714  
715  
716  
717  
718  
719  
720  
721  
722  
723  
724  
725  
726  
727  
728  
729  
730  
731  
732  
733  
734  
735  
736  
737  
738  
739  
740  
741  
742  
743  
744  
745  
746  
747  
748  
749  
750  
751  
752  
753  
754  
755  
756  
757  
758  
759  
760  
761  
762  
763  
764  
765  
766  
767  
768  
769  
770  
771  
772  
773  
774  
775  
776  
777  
778  
779  
780  
781  
782  
783  
784  
785  
786  
787  
788  
789  
790  
791  
792  
793  
794  
795  
796  
797  
798  
799  
800  
801  
802  
803  
804  
805  
806  
807  
808  
809  
810  
811  
812  
813  
814  
815  
816  
817  
818  
819  
820  
821  
822  
823  
824  
825  
826  
827  
828  
829  
830  
831  
832  
833  
834  
835  
836  
837  
838  
839  
840  
841  
842  
843  
844  
845  
846  
847  
848  
849  
850  
851  
852  
853  
854  
855  
856  
857  
858  
859  
860  
861  
862  
863  
864  
865  
866  
867  
868  
869  
870  
871  
872  
873  
874  
875  
876  
877  
878  
879  
880  
881  
882  
883  
884  
885  
886  
887  
888  
889  
890  
891  
892  
893  
894  
895  
896  
897  
898  
899  
900  
901  
902  
903  
904  
905  
906  
907  
908  
909  
910  
911  
912  
913  
914  
915  
916  
917  
918  
919  
920  
921  
922  
923  
924  
925  
926  
927  
928  
929  
930  
931  
932  
933  
934  
935  
936  
937  
938  
939  
940  
941  
942  
943  
944  
945  
946  
947  
948  
949  
950  
951  
952  
953  
954  
955  
956  
957  
958  
959  
960  
961  
962  
963  
964  
965  
966  
967  
968  
969  
970  
971  
972  
973  
974  
975  
976  
977  
978  
979  
980  
981  
982  
983  
984  
985  
986  
987  
988  
989  
990  
991  
992  
993  
994  
995  
996  
997  
998  
999  
1000

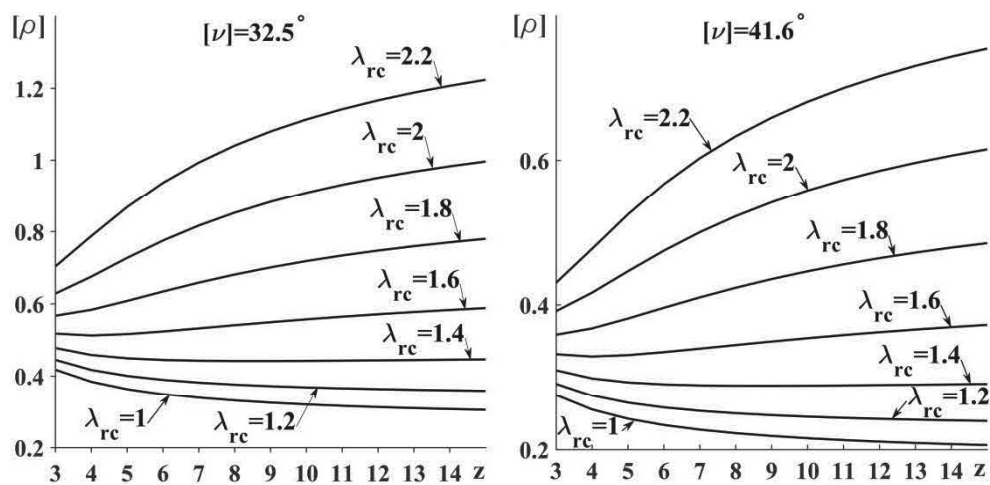


Figure 8. Dependence of the allowable curvature radius  $[\rho]$  of the cam profile on the number  $z$  of slots and limiting radius  $\lambda_{rc}$  in the zone IV

159x80mm (600 x 600 DPI)

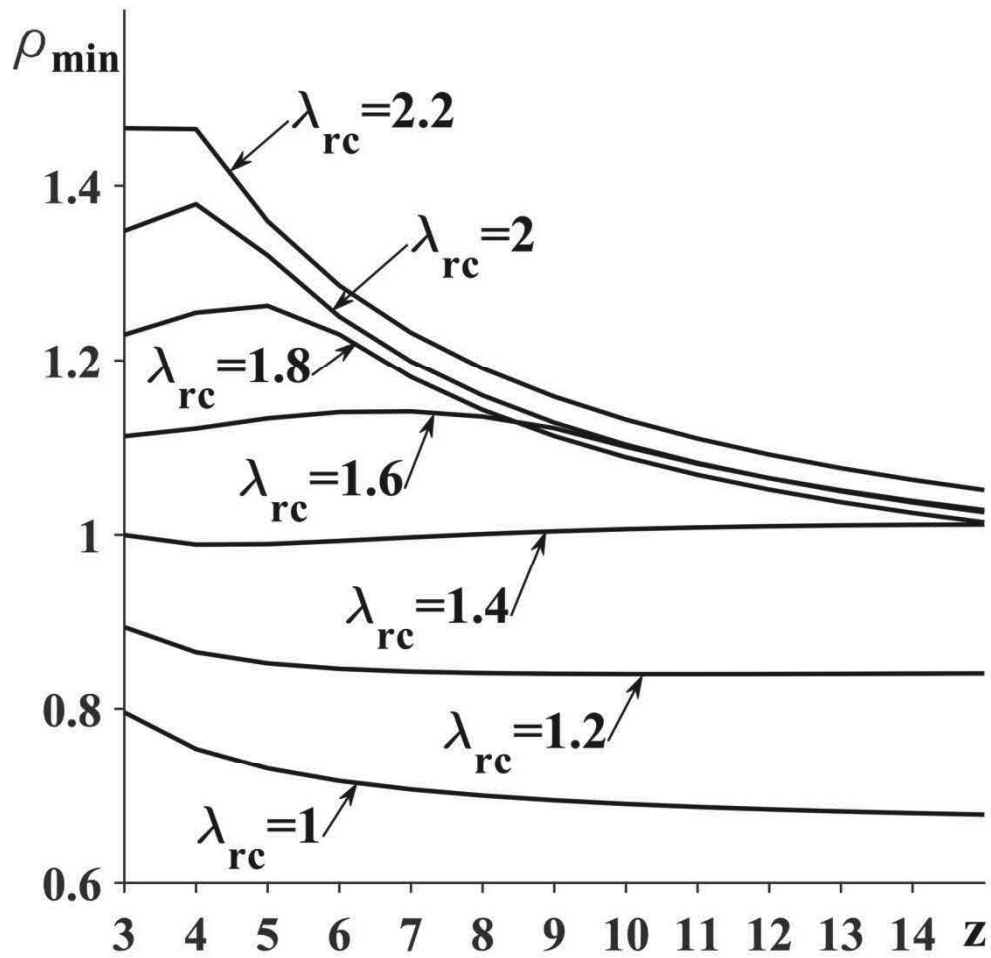


Figure 9. Dependence of the minimum curvature radius  $\rho_{\min}$  of the cam profile on the number  $z$  of slots and limiting radius  $\lambda_{rc}$  in the zone IV

80x80mm (600 x 600 DPI)

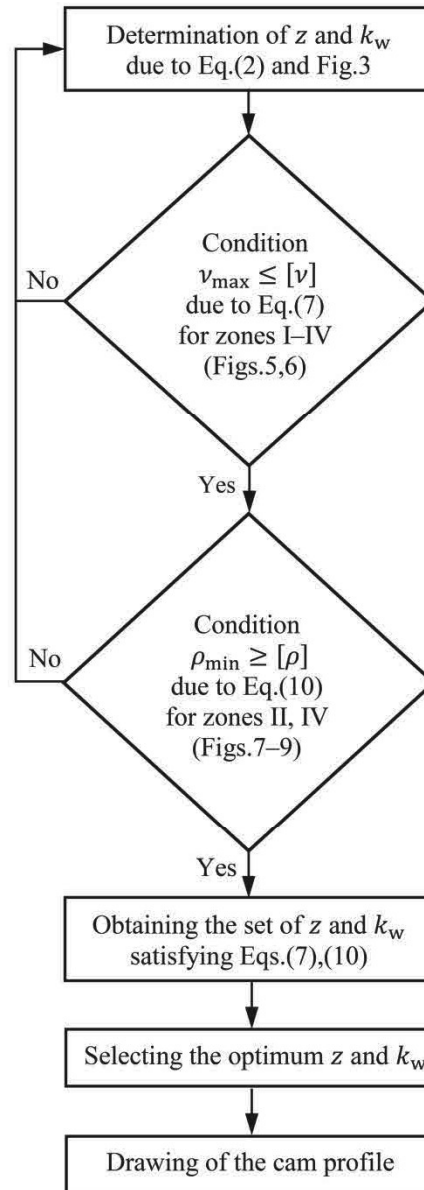


Figure 10. Synthesis algorithm for the groove cam Geneva mechanism

80x199mm (600 x 600 DPI)



1  
2  
3  
4  
5  
6  
7  
8  
9  
10  
11  
12  
13  
14  
15  
16  
17  
18  
19  
20  
21  
22  
23  
24  
25  
26  
27  
28  
29  
30  
31  
32  
33  
34  
35  
36  
37  
38  
39  
40  
41  
42  
43  
44  
45  
46  
47  
48

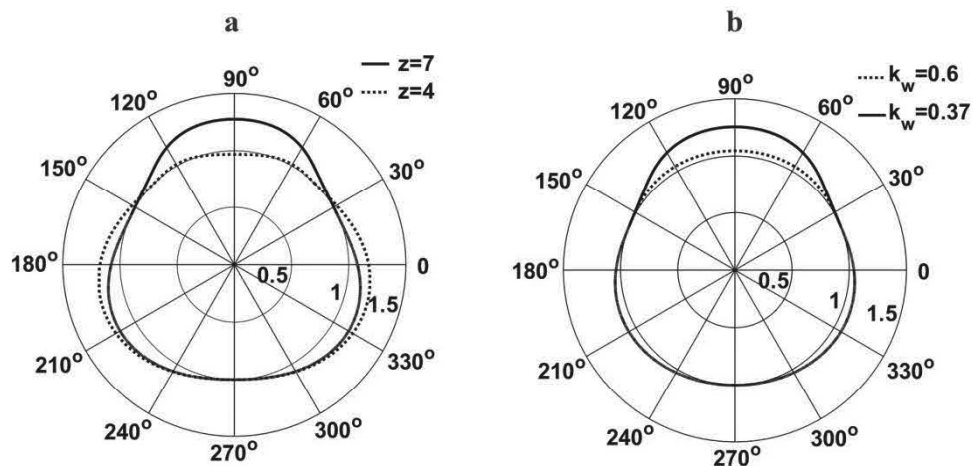


Figure 11. Synthesised paths of the driving pin: (a)  $k_w=0.3$ ; (b)  $z=8$

159x80mm (600 x 600 DPI)